TIME REVERSAL INVARIANCE AND UNIVERSALITY OF TWO DIMENSIONAL GROWTH PROCESSES

by

Damin Liu

B.Sc., University of Science and Technology of China, 1984

THESIS SUBMITTED IN PARTIAL FULFILLMENT OF

THE REQUIREMENTS FOR THE DEGREE OF

MASTER OF SCIENCE

in the Department

of

Physics

SIMON FRASER UNIVERSITY

March 1987

APPROVAL

Name: Damin Liu

Degree: Master of Science

Title of thesis: Time Reversal Invariance And Universality Of Two Dimensional Growth Processes

Examining Committee:

Chairman: M.L.W. Thewalt

M. Plischke
Senior Supervisor

D .H. Boal

R.H. Enns

L.E. Ballentine
External Examiner
Department of Physics
Simon Fraser University

Date Approved: Feburary 3, 1987

PARTIAL COPYRIGHT LICENSE

I hereby grant to Simon Fraser University the right to lend my thesis, project or extended essay (the title of which is shown below) to users of the Simon Fraser University Library, and to make partial or single copies only for such users or in response to a request from the library of any other university, or other educational institution, on its own behalf or for one of its users. I further agree that permission for multiple copying of this work for scholarly purposes may be granted by me or the Dean of Graduate Studies. It is understood that copying or publication of this work for financial gain shall not be allowed without my written permission.

Title of Thesis/Project/Extended Essay

Time Reversal and Universality of Two Dimensional Growth Processes

Author:

(signature)

LIU, Da-Min

(name)

April 13th, 1987

(date)

ABSTRACT

A model for the evolution of the profile of a growing and melting interface has been studied. The parameter of the model is the average net growth velocity v of the interface which is determined by the difference between the rates of deposition and evaporation. For the case of reversible growth (v=0) the problem is exactly solved by mapping the system onto a one-dimensional kinetic Ising model. For the irreversible growth (v≠0) Monte Carlo methods were employed to calculate the dynamic structure factor S(k,t) and the time correlation functions. It is found that S(k,t) obeys the dynamic scaling form : $S(k,t) \sim k^{-2+\eta} f(k^z t)$ with $\eta \simeq 0$ for all v. For v=0, z=2 and for v≠0 we obtained $z \simeq 3/2$ which is in excellent agreement with the previous numerical simulations and analytical results. The question of universality of dynamic growth processes is also discussed.

ACKNOWLEDGEMENTS

I would like to express my sincere thanks to Dr. M. Plischke for suggesting this topic and helping me go through the study to its completion. He spent a lot of time helping me to understand the subject and the theories related to it. He read through my thesis many times and made many suggestions and corrections which were extremely helpful to me. This work would not have been possible without his endless support and encouragement.

I am very grateful to Dr. Zoltan Rácz for having taken time to patiently explain to me things that I didn't understand. In addition, I wish to thank my supervisory committee for its help in my graduate studies.

The financial support provided by Simon Fraser University and the Natural Sciences and Engineering Research Council is also gratefully acknowledged.

DEDICATION

To my grandmother

TABLE OF CONTENTS

LIST OF FIGURES

CHAPTER I

INTRODUCTION

The physics of nonequilibrium processes is a rich branch of physics. Among the nonequilibrium processes are the aggregation of smoke particles (see Figure 1), colloid aggregation, dielectric breakdown, fluid displacement in porous media, crystal growth and many others.[1] An understanding of these nonequilibrium phenomena is certainly important theoretically and technologically.

Unfortunately our understanding of nonequilibrium phenomena is relatively limited in comparison to equilibrium phenomena at the present time. For example, the equilibrium properties of a thermodynamic system can be obtained quite satisfactorily from the basic assumptions of statistical mechanics. However, nonequilibrium properties are beyond this simple tool. Consider the processes we have mentioned above. Not only do we know little about the microscopic interactions controlling some of these processes, but also we are dealing with nonequilibrium processes. Although the equations describing these processes may be well defined, theoretical advance is hampered by the fact that the surfaces are highly convoluted, display large fluctuations and boundary conditions are changing with time. Another difficulty is the lack of knowledge of their spatial structures. Models have to be proposed to deal with these processes. It is found[1] that some nonequilibrium phenomena can be described in terms of models in which a single cluster grows

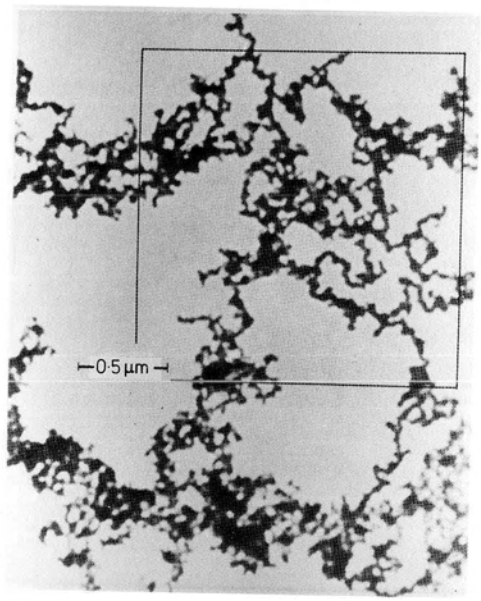

Figure 1: Transmission electron micrograph of an iron aggregate formed in smoke particle aggregation. Constituent particles are roughly 40Å in radius.

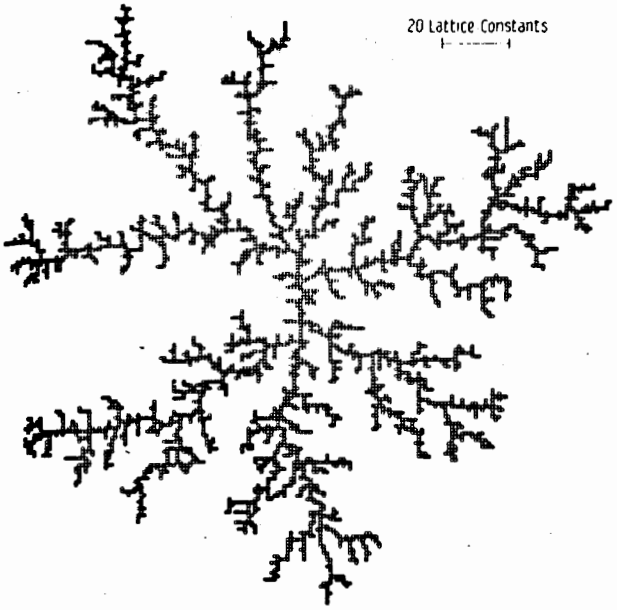

Figure 2: DLA aggregate of 3,000 particles on a square lattice.

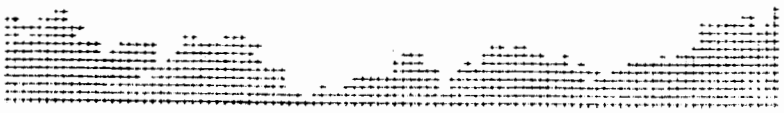

Figure 3: The Eden aggregate on a square lattice of L=96. The figure shows only the top rows, containing surface sites.

through the addition of individual particles. Two elementary and well studied growth models are the diffusion-limited aggregation (DLA) model[2] and the Eden model.[3] Several variants of these two models have also been proposed.

The DLA process was proposed by T.A. Witten and L.M. Sander.[2] The rules of the model are quite simple. One starts with a seed particle at the origin of a lattice. Another particle is allowed to walk at random (i.e. diffuse) from far away until it arrives at one of the lattice sites adjacent to the occupied site. There it is stopped and another particle is launched and halted when adjacent to an occupied site, and so forth. If a particle touches the boundaries of the lattice in its random walk it is removed and another introduced. An arbitrarily large cluster may be formed in this way. Figure 3 shows a 3,000-particle aggregate on a square lattice. One sees immediately the striking similarity with the smoke particle cluster of Figure 1.

The Eden model[3] is also very simple. The process is started by placing a seed particle on a lattice site. The cluster is then grown by adding particles at randomly selected unoccupied sites adjacent to the existing cluster. Alternatively one can consider the initial state to be a substrate of finite length or area and confine the growing cluster to a strip or a column. Figure 2 shows the surface configuration of particles accumulated on a strip of length L= 96 on a square lattice.

In both the DLA process and the Eden model, the algorithm is assumed without explicit reference to the details of the forces between the particles. The reason is that some features of aggregation processes are rather insensitive to the details of the particle-particle interaction. For example, very different processes such as dielectric breakdown[5] and smoke particle aggregation[6] have strong similarity in their spatial structures. It seems likely that at least the structures arising in aggregation processes can be understood without considering the details of the interaction. As we can see from Figure 2, the clusters grown by DLA are fractals, while those from the Eden algorithm are compact but have a rough surface.

The DLA process and its variants seem to describe very well a wide variety of phenomena which at first sight are unrelated such as the aggregation of smoke particles,[6] colloid aggregation[7] and dielectric breakdown.[5] The DLA process is diffusion controlled. The exposed ends of the cluster grow more rapidly than the interior because the added particles are captured, with high probability, before they reach the interior. The fractal dimension D of the DLA model is less than d,[2,4] where d is the Euclidean dimension of the space in which the process takes place. In studying the DLA process, the calculation or measurement of the fractal dimension D is important, since the density-density correlation function, the radius of gyration and the number of particles of the aggregate, etc. are all associated with D. For instance, the density-density correlation function of a fractal object is

described by the equation:

$$\langle \rho(\bar{r}+\bar{r}')\rho(\bar{r}')\rangle \sim r^{-A}$$

where < > denotes an ensemble average and the exponent A is related to D by D=d-A. A can be determined from the slope when one plots $\log\langle \rho(\bar{r}+\bar{r}')\rho(\bar{r}')\rangle$ vs log(r). In two dimensions, D is found to be about 1.7.[2] However, D is by no means the only exponent needed to describe the DLA process completely. As pointed by P. Meakin and T.A. Witten,Jr.,[8] DLA clusters have a characteristic scaling property besides their fractal dimension, namely the mass of the interface. Various measurements of this mass are consistent with each other. This mass in turn scales with a well-defined power δ of the size of the cluster. It seems likely that this power can not be expressed in a simple way in terms of the fractal dimension D of the aggregate and the dimension d of space. More recently Halsey, Meakin and Procaccia[9] have pointed out that an infinite number of exponents may be necessary for a complete description of such clusters. The fractal dimension is only the most obvious of these. At the present time the physical meaning and hence methods of determining the hierarchy of exponents are still unclear.

Some nonequilibrium processes may be described particularly well by the DLA model. The smoke particle aggregation process is one of them. The aggregates studied by Forrest and Witten[6] were formed when a melted vapor produced by heating a plated filament condensed. The particles--approximately 40Å in radius--accumulated in a thin spherical shell of roughly 1cm radius.

Then they drifted down to a transmission electron microscope (TEM) slide where a photo of the aggregate was taken (see Figure 1). The technique described above can of course be used and was actually used to analyze the photograph of the aggregate. The result $D \simeq 1.7$ is in excellent agreement with that calculated from the DLA model.

DLA clusters, and fractals in general, are scale invariant. The criterion for scale invariance one may use is that in a scale invariant object correlation functions are unchanged up to a constant under rescaling of lengths by an arbitrary factor b:

$$<\rho(b\vec{r}_1)\rho(b\vec{r}_2)> \simeq b^{-A}<\rho(\vec{r}_1)\rho(\vec{r}_2)>$$

this is only another form of

$$<\rho(\vec{r}+\vec{r}')\rho(\vec{r}')> \sim r^{-A}$$

which has been proven true. This means that each part of the aggregate, statistically speaking, is similar to the whole. The aggregate has no natural length scale.

Scale invariance is most familiar to us in the context of critical phenomena in equilibrium thermodynamic systems. In equilibrium thermodynamics the critical properties of many seemingly different systems are determined only by the general features of the systems such as the spatial dimensionality, the symmetry of the Hamiltonian and the symmetries of the equation of motion. This notion became known as the universality hypothesis. The universality hypothesis has been verified experimentally for fluids and magnetic systems. Since there is

empirical evidence that power law behavior is found even in nonequilibrium processes, one can ask whether the concept of universality applies in these situations and, if so, what the important features of the dynamical processes are that determine the universality class of a system.

If the DLA process obeys the universality hypothesis, its properties should not depend on the lattice on which the cluster grows and the details of growth rules. Indeed, simulations of the DLA process on the square lattice, on the triangular lattice on no lattice at all and that of a partly absorbing modified DLA process show that the universality hypothesis holds for the DLA model.[4]

The Eden process is often used to simulate biological growth processes and crystal growth. It is quite different from DLA and one of the essential differences is the compactness of the spatial structures. There is evidence from simulations that the process is space filling and its fractal dimension is the same as the Euclidean dimension.[10,11] Therefore, in the Eden model and its variants, the evolution of the surface of the aggregates is probably the most interesting quantity since the resulting clusters are compact. It is easily seen from Figure 3 that the surface is rough. The roughness was first measured in spherical geometry by M. Plischke and Z.Rácz.[11,12] The width of the surface is found to behave as $\xi_N \sim N^{\bar{\nu}}$ where N is the number of particles in the cluster, while the mean radius of the cluster scales as $\bar{r}_N \sim N^{\nu} \sim N^{1/d}$ in both two dimensional and three

dimensional cases. Here d is again the Euclidean dimension of the space in which the process occurs. M. Plischke and Z. Rácz found that $\bar{\nu}<\nu$, indicating the presence of a second diverging length in the Eden model. R. Jullien and R. Botet first studied the Eden model in a strip geometry. Their result for $\bar{\nu}/\nu$ in the two dimensional case is 0.3±0.03, giving evidence to the inequality $\bar{\nu}<\nu$. The evolution of the surface of two-dimensional Eden deposits grown in a strip of width L was also studied by M. Plischke and Z. Rácz.[14] The advantage of the strip geometry is that it provides a convenient separation of control parameters. The width L of the strip and the average height $\bar{h}$ of the surface, or, in appropriate units, the time of the growth $t\sim\bar{h}$ can be varied independently. Therefore, one can study the effects of changing L and $\bar{h}$ separately which is impossible in spherical geometry where the cluster starts growing from a seed particle and a single parameter N, the number of particles in the cluster, controls both the "height", i.e. the mean radius $\bar{r}_N\sim N^{\nu}\sim N^{1/d}$, and the strip "width". One expects that curvature effects are negligible for $N\to\infty$.

The scaling properties of Eden clusters in spherical geometry can be obtained from those in strip geometry. For example, in strip geometry the width of the surface is known to have the scaling form $\xi(L,t)\sim L^{\chi}G(t/L^{z})$ with $G(x)\to$const as $x\to\infty$ and $G(x)\sim x^{\chi/z}$ as $x\to 0$, where χ and z are constant exponents when d is fixed. For a cluster growing in a spherical geometry with a radius $\bar{r}_N\sim\bar{h}\sim t\sim L$ the width of the surface behaves as

$\xi(\bar{r}_N,t) \sim \bar{r}_N^{\chi} G(t/\bar{r}_N^{z})$. If $\bar{r}_N \sim N^{\nu}$ and $z>1$ we have $\xi_N \sim N^{\bar{\nu}}$ with $\bar{\nu}=\chi\nu/z=\chi/dz$. In the two dimensional model, χ and z are found to be 1/2 and 1.55±0.15, respectively. This also supports $\bar{\nu}<\nu$.

The question of whether the universality hypothesis holds for the Eden process can also be asked although the Eden model does not have very obvious scale invariance property. For instance, one can ask: are χ and z in $\xi(L,t)\sim L^{\chi}G(t/L^{z})$ universal ? Besides computer simulations of the two dimensional Eden model, analytical analysis of a model differential equation was carried out[15] which gave $\chi=1/2$ and $z=3/2$, in excellent agreement with numerical results mentioned earlier in this thesis.

The dynamic scaling form $\xi(L,t)\sim L^{\chi}G(t/L^{z})$ and the value of χ and z are also regained by studying the "ballistic deposition" model. There are also a number of simulations confirming that for a strip geometry the width scales as L^{χ} as $t\rightarrow\infty$ with $\chi=1/2$.[12,13,14,16,17] These results coming from different models seem to support the universality hypothesis. Within the Eden model itself, it has been conjectured[18] that $\chi=1/2$ and $z=3/2$ may apply even for d=3 and higher dimensions. This superuniversality of the Eden model is still to be confirmed numerically or analytically.

Besides the above universality class, $\chi=1/2$ and $z=3/2$, another class with $\chi=1/2$ and $z=2$ was also found in Kardar *et al.*'s renormalization group calculation.[15] Long before this work the same universality class was obtained by S.F. Edwards

and D.R. Wilkinson.[19] Comparing these two theories we see that Kardar *et al.*'s model is an improvement over the Edwards and Wilkinson model which already contains the essential features of the deposition process. Both groups started from the Langevin equation for local growth of the profile:

$$\frac{\partial h(\bar{x},t)}{\partial t}=\nu^*\nabla^2 h(\bar{x},t)+\frac{\lambda^*}{2}(\nabla h(\bar{x},t))^2+\eta(\bar{x},t)$$

where $h(\bar{x},t)$ is the height of the profile measured from an appropriately chosen reference level and $\eta(\bar{x},t)$ represents the noise. Edwards and Wilkinson studied the case in which $\lambda^*=0$. The universality class $\chi=1/2$ and $z=3/2$ corresponds to the case in which $\lambda^*\neq 0$. The nonlinear term $\frac{\lambda^*}{2}(\nabla h(\bar{x},t))^2$ seems to play an essential role in driving the system from one universality class to the other.

It is important to understand what kind of features of the system underlie the universality class change. For nonequilibrium processes, if the universality hypothesis holds, one may classify simple growth processes according to general features of the processes. To calculate critical exponents only highly idealized models which contain the relevant features of the growth processes are needed.

In this thesis, we study a simple two dimensional model of interface dynamics which describes a surface tension biased process of simultaneous deposition and evaporation of particles. The model is so simple that it can be treated analytically, at least in one special case, and large simulations can be carried

out. This model helps us to understand the role of the nonlinear term and gives support to the universality hypothesis. This model has two universality classes. The change from one class to the other is controlled by the average translational velocity v of the interface. In the equilibrium case (v=0), the growth algorithm is microscopically time reversible and an exact solution leads to the exponents $\chi=1/2$ and $z=2$. When $v\neq 0$ and time reversal symmetry is broken, an exact solution is no longer possible. Monte Carlo simulations were carried out for both reversible and irreversible processes of the model. For irreversible cases, simulations yield $\chi=1/2$ and $z=3/2$ which are consistent with results from other irreversible models, while for the reversible case, simulations yield $\chi=1/2$ and $z=2$. The change of z from 2 to 3/2, i.e. the change from one universality class to the other, can thus be interpreted as being due to the breaking of time reversal symmetry.

1.1 Model

We consider here the simple case of a square lattice with a as the lattice constant (a=1 for convenience). The sites of the lattice may be occupied by particles of radius $\sqrt{2}$. The motion of the surface is restricted to an infinite strip in the (1,1) direction of the square lattice. We assume periodic boundary condition in the direction perpendicular to the strip. The initial configuration is chosen as shown in Figure 4.

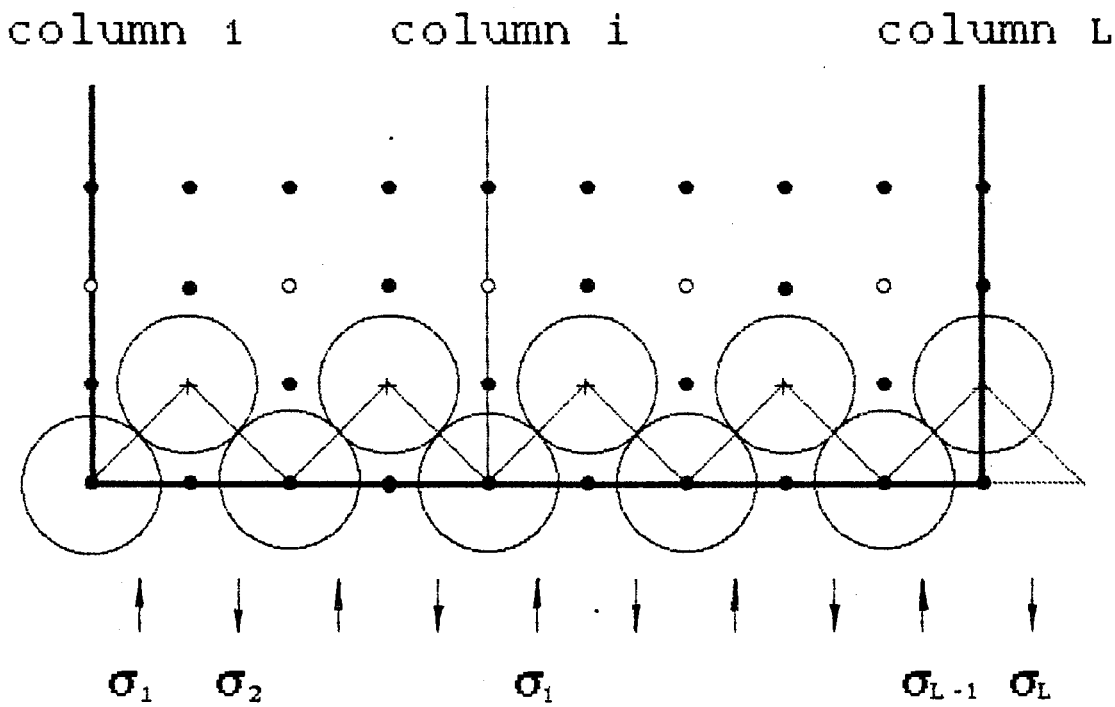

Figure 4: The initial configuration of the model. Circles represent particles. Deposition occurs randomly at one of the valleys, thus the sites marked by o are eligible deposition sites. Particles marked by + are eligible to evaporate.

The dynamics is introduced into the model by depositing and annihilating particles at eligible sites on the surface. Local minima of the surface are eligible sites for deposition and local maxima of the surface are eligible sites for evaporation (see Figure 4). The algorithm restricts the heights of neighboring columns to differ only by +1 or -1. The constraint that deposition and evaporation takes place only at valleys and peaks is similar to a surface tension.

Particles are deposited or evaporated one at a time with a time interval τ between events. Time is measured from the beginning of the process, thus $t=t_n=n\tau$, where n is the number of particles deposited and evaporated from the start of the process. At time $n\tau$ either a new particle is added to an eligible site on the surface or a particle at an eligible site is evaporated. The probabilities of deposition and evaporation are P_+ and P_- ($P_+ + P_- = 1$) respectively and the site where the event takes place is selected randomly from all the eligible sites. This model may simulate molecular exchange between solid and vapor phases.

The model can be mapped onto a one dimensional kinetic Ising model. Let's connect all the nearest neighbor surface sites with bonds and denote the slope of the ith bond by σ_i (see Figure 4). Obviously σ_i is either +1 or -1 depending on whether the bond goes up or down. To each surface configuration corresponds a set of σ_i ($i=1,2,\ldots\ldots,L$), denoted by $\{\sigma_i\}$. Hence we have converted the surface configuration into a set of two state variables at

any given time t_n, and the system can then be treated as a kinetic Ising model.

Note that for the periodic boundary condition to be valid at all time, L has to be an even integer and σ_i (i=1,2,.....,L) are not all independent of each other. It is always true that

$$\sum_{i=1}^{L} \sigma_i(t_n)=0 \qquad \text{for all n} \tag{1.1.1}$$

The rate of deposition or evaporation at time t at column i can now be expressed as:

$$w_i=\frac{P_+}{4\tau}(1-\sigma_i)(1+\sigma_{i+1})+\frac{P_-}{4\tau}(1+\sigma_i)(1-\sigma_{i+1})$$

$$=[1-\sigma_i\sigma_{i+1}+\lambda(\sigma_{i+1}-\sigma_i)] \tag{1.1.2}$$

where τ is a constant which sets the time scale and

$$\lambda=P_+-P_-=2P_+-1 \tag{1.1.3}$$

Although we shall be working with this model throughout this thesis, generalization to other lattices and higher dimension should be obvious from the construction. It is not, however, possible to express the surface configuration in terms of Ising spins in arbitrary dimension and on any given lattice.

1.2 Quantities to be calculated

Nonequilibrium processes reach a steady state in a long period of time. We are interested in steady state properties as well as dynamic properties of systems. Steady state properties

are usually easier to obtain analytically than dynamic properties. We shall give an example of how an equilibrium model--the two dimensional solid-on-solid (SOS) model--can be treated analytically, but first we introduce a few quantities--the width of the surface $\xi(L,t)$, the structure factor $S(k,t)$, the relaxation function $\Psi(k,t)$ and time correlation function $\Phi(k,\tau)$.

A) The width of the surface $\xi(L,t)$;

For compact models, one of the easiest and most interesting quantities is probably the width $\xi(L,t)$ of the surface zone. For a particular configuration $\{h\}=\{h_i(t_n)\}$, ξ^2 is defined as

$$\xi^2(\{h\},L,t_n)=\frac{1}{L}\sum_{i=1}^{L}[h_i(\{h\},t_n)-\bar{h}(\{h\},t_n)]^2$$

$$=\overline{h_i(\{h\},t_n)^2}-\bar{h}(\{h\},t_n)^2 \qquad (1.2.1)$$

where $\overline{(\ )}$ denotes the average of ( ) over L.

Let the distribution function be $P(\{h\},L,t_n)$ and $<\ >$ denote the average over $P(\{h\},L,t_n)$. The macroscopic quantity ξ^2 is then defined as the average of $\xi^2(\{h\},L,t_n)$ over all possible configurations:

$$\xi^2(L,t)=<\xi^2(\{h\},L,t_n)>$$

$$=\sum_{\{h\}}\xi^2(\{h\},L,t_n)P(\{h\},L,t_n)$$

$$=\overline{h_i(t_n)^2}-\bar{h}(t_n)^2 \qquad (1.2.2)$$

B) The structure factor S(k,t);

A more detailed characterization of the surface can be obtained by decomposing the surface into Fourier modes and investigating the static and dynamic properties of these modes.

Define

$$\hat{h}(k,t)=\frac{1}{\sqrt{L}}\sum_{j=1}^{L}[h_j(t)-\bar{h}(t)]e^{ikj}$$

for a particular configuration, with

$$k=2n\pi/L, \qquad n=0,\pm1,\pm2,.....,\pm(L/2-1),L/2$$

Hence (1.2.2) can be rewritten as

$$\xi^2(L,t)=\frac{1}{L}\sum_{k}S(k,t) \qquad (1.2.3)$$

where

$$S(k,t)=<\hat{h}(k,t)\hat{h}(-k,t)> \qquad (1.2.4)$$

The quantity S(k,t) is called the dynamic structure factor.

C) The relaxation function $\Psi(k,t)$ and the time correlation function $\Phi(k,\tau)$;

The evolution of the surface is expected to become stationary and $\xi^2(L,t)$ and S(k,t) become time independent in the long time limit. The behavior of $\xi^2(L,t)$ and S(k,t) must be quite different for stationary state and far-from-stationary state. The far-from-stationary state dynamics can be studied by investigating the relaxation function

$$\Psi(k,t)=\frac{S(k,\infty)-S(k,t)}{S(k,\infty)-S(k,0)} \qquad (1.2.5)$$

The decay of fluctuations in the stationary state can be characterized by the time correlation function

$$\Phi(k,\tau)=\lim_{t\to\infty}\frac{1}{S(k,t)}<\hat{h}(k,t+\tau)\hat{h}(-k,t)> \qquad (1.2.6)$$

The Hamiltonian of the simplest two dimensional SOS model is given by

$$H=\epsilon\sum_{i=1}^{L}(h_{i+1}-h_i)^2 \qquad (1.2.7)$$

where ϵ is a constant and h_i is the height of column i of a strip of length L.

We assume periodic boundary conditions and Fourier transform h_i

$$h_j=\frac{1}{\sqrt{L}}\sum_k \hat{h}(k)e^{ikj}$$

$$\hat{h}(k)=\frac{1}{\sqrt{L}}\sum_j^{L} h_j e^{-ikj}$$

$$(k=2n\pi/L \qquad n=0,\pm1,\pm2,\ .....,\pm(L/2-1),L/2)$$

We thus have

$$H=\epsilon\sum_{i=1}^{L}(h_{i+1}-h_i)^2=\sum_{k\neq0}\epsilon(k)\hat{h}(k)\hat{h}(-k) \qquad (1.2.8)$$

where $\epsilon(k)=2\epsilon(1-\cos k)$.

From the law of equipartition of energy we obtain

$$\epsilon(k)<\hat{h}(k)\hat{h}(-k)>=K_B T/2 \qquad (1.2.9)$$

where K_B is the Boltzmann constant and < > denotes the average over the ensemble.

Therefore, the square of the width of the surface is

$$\xi^2(L,T)=\frac{1}{L}<\sum_{i=1}^{L}(h_i-\bar{h})^2> =\frac{1}{L}\sum_{k\neq 0}<\hat{h}(k)\hat{h}(-k)> \qquad (1.2.10)$$

For large L and small k, $\epsilon(k)\sim k^2$, hence (1.2.9) becomes

$$<\hat{h}(k)\hat{h}(-k)>\sim k^{-2+\eta} \qquad \text{with } \eta=0$$

And (1.2.10) is

$$\xi^2(L,T)\sim \frac{1}{L}\sum_{k\neq 0}\frac{1}{k^2} \sim \int_{2\pi/L}^{\infty}\frac{1}{k^2}\,dk \sim L$$

$$\xi(L,T)\sim L^{1/2}$$

The surface is rough as $L\to\infty$ (or, equivalently, $k\to 0$ in momentum space) and the limit $L\to\infty$ may be considered a critical point of the system.

Now suppose we assume that dynamics is modeled by

$$\frac{\partial h_i(t)}{\partial t} = -\frac{\Gamma}{2}\frac{\partial H}{\partial h_i} +\eta_i(t)$$

$$=\Gamma\epsilon(h_{i+1}+h_{i-1}-2h_i)+\eta_i(t)$$

where Γ is a constant, $\eta_i(t)$ is noise with $<\eta_i(t)>=0$ and $<\eta_i(t)\eta_j(t')>= 2D\delta_{ij}\delta(t-t')$, and the average is the average over the noise.

Fourier transforming $\eta_i(t)$ and $h_i(t)$, we obtain

$$h_i(t)= \frac{1}{\sqrt{L}} \sum_k \hat{h}(k,t)\ e^{ikj}$$

$$\eta_i(t)= \frac{1}{\sqrt{L}} \sum_k \hat{\eta}(k,t)\ e^{ikj}$$

Consequently, we have

$$\frac{d\hat{h}(k,t)}{dt} = -\Gamma\epsilon(k)\hat{h}(k,t)+\hat{\eta}(k,t)$$

where $\epsilon(k)= 2\epsilon(k)(1-\cos k)$.

It is easy to obtain that $<\hat{\eta}(k,t)>=0$ and $<\hat{\eta}(k_1,t_1)\hat{\eta}(k_2,t_2)>= 2D\delta_{k_1,-k_2}\delta(t_1-t_2)$.

We solve this equation and obtain

$$\hat{h}(k,t) =\int_0^t dt'\ e^{-\Gamma\epsilon(k)(t-t')}\hat{\eta}(k,t')\ +\hat{h}(k,0)\ e^{-\Gamma\epsilon(k)t}$$

For simplicity, we assume that we start the process from a flat substrate, thus $\hat{h}(k,0)=0$. Therefore, we have, assuming $t_2>t_1$

$$<\hat{h}(k_1,t_1)\hat{h}(k_2,t_2)>= \frac{D}{\Gamma}\delta_{k_1,-k_2}\cdot$$

$$(e^{-\Gamma\epsilon(k_1)(t_2-t_1)}\ -e^{-\Gamma\epsilon(k_1)(t_1+t_2)})/\epsilon(k_1)$$

This yields that for small k (thus $\epsilon(k)\simeq k^2$),

$$S(k,t)=<\hat{h}(k,t)\hat{h}(-k,t)>$$

$$\simeq \frac{D}{\Gamma}(1-e^{-2\Gamma k^2 t})/k^2$$

$$\sim k^{-2}f(k^2t)$$

and

$$\Psi(k,t)=\frac{S(k,\infty)-S(k,t)}{S(k,\infty)-S(k,0)}\simeq e^{-2\Gamma k^2 t}$$

and

$$\Phi(k,\tau)=\lim_{t\to\infty}\frac{1}{S(k,t)}<\hat{h}(k,t+\tau)\hat{h}(-k,t)>\simeq e^{-\Gamma k^2\tau}$$

Since there is no mechanism that restricts the long wavelength fluctuations, one expects that the fluctuations diverge as L approaches infinity. Thus $L\to\infty$ can be regarded as a critical point. This critical point should also be reflected in the structure factor as a singular point. The small k-vector long time limit of the structure factor may be analyzed in terms prescribed by dynamic scaling theory for finite size systems:

$$S(k,t)\sim k^{-2+\eta}f(k^z t) \qquad (1.2.11)$$

where the static (η) and dynamic (z) exponents determine the universality class the model belongs to.

Therefore the calculation above gives us explicitly the dynamic scaling forms and the dynamic exponent z=2.

We know that in the two dimensional Eden model on a strip of length L the width of the surface of the cluster behaves as

$$\xi(L,t)\sim L^{\chi}G(t/L^z) \qquad (1.2.12)$$

where $G(x)\to$const as $x\to\infty$ and $G(x)\sim x^{\chi/z}$ as $x\to 0$.
That is

$$\xi(L,t)\sim L^{\chi} \qquad (t\to\infty, \text{ steady state})$$

and

$$\xi(L,t)\sim t^{\chi/z} \qquad (t\rightarrow 0, \text{dynamic})$$

This power law behavior of dynamic and static states of the process resembles the power law behavior in the critical phenomena in equilibrium thermodynamics.

In the following chapters we shall be examining our model by studying the width of the surface, the structure factor $S(k,t)$ the relaxation function $\Psi(k,t)$ for far-from-stationary state dynamics and the time correlations $\Phi(k,\tau)$ in the stationary state. The Fourier decomposition method described in the example is used. The analysis, in terms of a Fourier decomposition, is not obvious. We are assuming that the system has normal modes which can be indexed by k. This does not have to be true since no Hamiltonian such as (1.2.7) describes this model. In any case, this analysis turns out to be very helpful.

It is easily seen that overhangs are excluded in our model. Therefore when measured from a chosen reference level, the height of the surface is single valued. Any configuration of the aggregate can be uniquely expressed by the height $h_i(t_n)$ of all the columns, where $h_i(t_n)$ is given by

$$h_i(t_n)= \sum_{m=1}^{i} \sigma_m(t_n)+ h_o(t_n) \qquad (i=1,2,.....,L) \qquad (1.2.13)$$

where $h_o(t_n)$ is a constant at time t_n and where we have chosen the average height of the initial state as the reference level.

Once $h_i(t_n)$ is measured in Monte Carlo simulations or calculated analytically, various properties of the surface can be obtained. We present the results of our simulations of these quantities in Chapter III and first discuss the exactly solvable reversible case of the model.

CHAPTER II

ANALYTICAL ANALYSIS

In order to derive analytical results it is convenient to work with the continuous time version of our model. In the continuous time version, time t is taken as a continuous variable. However, the time scale can be related to that of the discrete case by equating the average number of particles deposited or evaporated during period t to the number of those during period t_n in the discrete model:

$$\langle n(t)\rangle = \int_0^t \sum_{i=1}^{L} \langle W_i(t')\rangle dt' = n(t_n) = t_n/\tau \tag{2.1}$$

The continuous time version can be described by the probability distribution $P(\{h\},t)$ and is defined through the master equation:

$$\frac{\partial P(\{h\},t)}{\partial t} = -\sum_{i=1}^{L} W_i(\{h\})P(\{h\},t) + \sum_{i=1}^{L} W_i(\{h\}_i)P(\{h\}_i,t) \tag{2.2}$$

where $\{h\}_i$ is the configuration right before the deposition or evaporation of a particle at column i (i=1,2,...,L). The profile {h} of the surface can be expressed in terms of Ising spins by (1.2.13). The master equation (2.2) then becomes an equation for the probability distribution $P_I(\{\sigma\},t)$ of the Ising states.

$$\frac{\partial P_I(\{\sigma\},t)}{\partial t} = -\sum_{i=1}^{L} W_i^{(I)}(\{\sigma\})P_I(\{\sigma\},t) + \sum_{i=1}^{L} W_i^{(I)}(\{\sigma\}_i)P_I(\{\sigma\}_i,t) \tag{2.3}$$

where $\{\sigma\}_i$ and $\{\sigma\}$ differ by a flip at site i (if allowed), and $W_i^{(I)}$ is given by (1.1.2)

$$W_i^{(I)}(\{\sigma\}) = \frac{1}{4\tau}[1-\sigma_i\sigma_{i+1}+\lambda(\sigma_{i+1}-\sigma_i)] \tag{2.4}$$

A deposition or evaporation at site i involves two "spins", $(\sigma_i,\sigma_{i+1})\rightarrow(-\sigma_i,-\sigma_{i+1})$ since in our model a deposition or evaporation of a particle requires so. Therefore, the allowed spin flip processes conserve the magnetization.

Inserting (2.4) into (2.3), we thus obtain

$$\frac{\partial P_I(\{\sigma\},t)}{\partial t} = -\sum_i \frac{1}{4\tau}[1-\sigma_i\sigma_{i+1}+\lambda(\sigma_{i+1}-\sigma_i)]P_I(\{\sigma\},t)$$

$$+\sum_i \frac{1}{4\tau}[1-\sigma_i\sigma_{i+1}-\lambda(\sigma_{i+1}-\sigma_i)]P_I(\sigma_1,\ldots,-\sigma_i-\sigma_{i+1},\ldots,\sigma_L,t) \tag{2.5}$$

where $(\sigma_1,\ldots,-\sigma_i,-\sigma_{i+1},\ldots,\sigma_L)$ is $\{\sigma\}_i$ mentioned above.

We shall show later that the width of the surface region $\xi(L,t)$ and the structure factor $S(k,t)$ can be expressed in terms of spin-spin correlation functions and we therefore concentrate on a derivation of these correlation functions by solving the master equation (2.5).

The spin-spin correlation functions are defined as

$$\sum_{\{\sigma\}} \sigma_j\sigma_{j+m}P(\{\sigma\},t) \tag{2.6}$$

As above we denote the correlation functions by $\langle\sigma_j\sigma_{j+m}\rangle$.

Simply, we denote

$$g_{j,m}(t) = \langle \sigma_j \sigma_{j+m} \rangle \qquad \text{for any } j,m$$

$$g_{j,0} = \langle \sigma_j \sigma_j \rangle = 1 \tag{2.7}$$

Multiplying (2.5) by $\sigma_j \sigma_{j+m}$, and summing over all possible $\{\sigma\}$, we get

$$\frac{\partial g_{j,m}(t)}{\partial t} = -\sum_{i,\{\sigma\}} \frac{1}{4\tau}[1-\sigma_i\sigma_{i+1}+\lambda(\sigma_{i+1}-\sigma_i)]P(\{\sigma\},t)\sigma_j\sigma_{j+m}$$
$$+\sum_{i,\{\sigma\}} \frac{1}{4\tau}[1-\sigma_i\sigma_{i+1}-\lambda(\sigma_{i+1}-\sigma_i)]P(\sigma_1,\ldots,-\sigma_i-\sigma_{i+1},\ldots,\sigma_L t)\sigma_j\sigma_{j+m} \tag{2.8}$$

It is easy to show that for $m \neq 1, L-1$ (2.8) becomes

$$\tau\frac{\partial g_{j,m}(t)}{\partial t} = -2g_{j,m}(t) + \tfrac{1}{2}\langle\sigma_{j+1}\sigma_{j+m}\rangle + \tfrac{1}{2}\langle\sigma_j\sigma_{j+m+1}\rangle$$
$$+ \tfrac{1}{2}\langle\sigma_{j-1}\sigma_{j+m}\rangle + \tfrac{1}{2}\langle\sigma_j\sigma_{j+m-1}\rangle$$
$$+ \tfrac{\lambda}{2}\langle\sigma_j\sigma_{j+m}\sigma_{j-1}\rangle + \tfrac{\lambda}{2}\langle\sigma_j\sigma_{j+m}\sigma_{j+m-1}\rangle$$
$$- \tfrac{\lambda}{2}\langle\sigma_j\sigma_{j+m}\sigma_{j+1}\rangle - \tfrac{\lambda}{2}\langle\sigma_j\sigma_{j+m}\sigma_{j+m+1}\rangle \tag{2.9a}$$

and for $m=1$

$$\tau\frac{\partial g_{j,1}(t)}{\partial t} = -g_{j,1}(t) + \tfrac{1}{2}\langle\sigma_{j-1}\sigma_{j+1}\rangle + \tfrac{1}{2}\langle\sigma_j\sigma_{j+2}\rangle$$
$$+ \tfrac{\lambda}{2}\langle\sigma_{j-1}\sigma_j\sigma_{j+1}\rangle + \tfrac{\lambda}{2}\langle\sigma_j\rangle$$
$$- \tfrac{\lambda}{2}\langle\sigma_{j+1}\rangle - \tfrac{\lambda}{2}\langle\sigma_j\sigma_{j+1}\sigma_{j+2}\rangle \tag{2.9b}$$

In the case of equilibrium growth ($\lambda=0$), equations (2.9a,b) contain only two-spin correlation functions and this makes the

problem solvable as we shall show below. For nonequilibrium growth ($\lambda \neq 0$) the three-spin correlation functions appearing on the right hand side do not, in general, cancel with each other, and equations (2.9a,b) are not exactly solvable. We shall return to the nonequilibrium case, but the exactly solvable case of $\lambda=0$ will be discussed first.

1) $\lambda=0$ ($v=0$) equilibrium growth

We have used the term "equilibrium" in the text. By this we mean that the average growth velocity is equal to zero. The average velocity is defined by $\bar{h}(t_n)/t_n$ in our discrete model, where $\bar{h}(t_n)$ is the mean height of the surface at time t_n and is obtained through the following formula

$$\bar{h}(t_n)=\frac{1}{L}\sum_{i=1}^{L}\langle h_i(t_n)\rangle = 2(P_+-P_-)n(t_n)= \lambda(2t_n/\tau) \qquad (2.10)$$

where again we have chosen the average height of the initial state as the reference level. In the continuum version the same result is given since we have related the continuum version to the discrete model by (2.1).

Because of (1.1.1) and (2.4), (2.1) becomes

$$\int_0^t \sum_{i=1}^{L} \frac{1}{4\tau}[1-\sigma_i(t')\sigma_{i+1}(t')]dt' = t_n/\tau \qquad (2.11)$$

while in the continuum model

$$\bar{h}(t_n)=\int_0^t \sum_{i=1}^{L} [W(\sigma_i,\sigma_{i+1})-W(-\sigma_i,-\sigma_{i+1})]dt'$$

$$=2\int_0^t \sum_{i=1}^{L} \frac{\lambda}{4\tau}(1-\sigma_i\sigma_{i+1})dt'$$

$$=2\lambda t_n/\tau \qquad (2.12)$$

It is clear from (2.10) and (2.12) that unless $P_+=1/2$ (and consequently, $\lambda=0$) the surface moves on the average with a non-zero velocity.

Due to the periodic boundary conditions, we have translational invariance of the correlation functions in the equilibrium case. That is

$$\langle\sigma_j\sigma_{j+m}\rangle = \langle\sigma_{j'}\sigma_{j'+m}\rangle \qquad \text{for all } j,j' \text{ and } m \qquad (2.13)$$

and obviously,

$$\langle\sigma_j\sigma_j\rangle = 1 \qquad (2.14)$$

Therefore we may simply denote $g_{j,m}$ by g_m. Letting λ be zero and using translational invariance, we obtain from (2.9) and (2.7) that

$$\begin{aligned}
\tau\frac{\partial g_m(t)}{\partial t} &= g_{m+1}(t)+g_{m-1}(t)-2g_m(t) \qquad (m\neq 1,L-1)\\
\tau\frac{\partial g_1(t)}{\partial t} &= g_2(t)-g_1(t) \qquad (2.15)\\
\tau\frac{\partial g_{L-1}(t)}{\partial t} &= g_{L-2}(t)-g_{L-1}(t)\\
g_0(t) &= 1
\end{aligned}$$

Note that $g_{L-i}(t)=g_i(t)$ due to periodic boundary conditions. In particular, $g_1(t)=g_{L-1}(t)$. Thus

$$\tau\frac{\partial g_1(t)}{\partial t} = g_2(t)-g_1(t) = g_2(t)+g_{L-1}(t)-2g_1(t)$$

$$\tau\frac{\partial g_{L-1}(t)}{\partial t} = g_{L-2}(t)-g_{L-1}(t) = g_{L-2}(t)+g_1(t)-2g_{L-1}(t) \tag{2.16}$$

With this substitution the L-1 equations (2.15) are now all of the same form.

If we ignore the trivial correlation function $g_0(t)$, we can consider the L-1 functions $g_1,\ldots,g_{L-1}$ to be periodic with periodicity L-1 so that the left nearest neighbor and the right nearest neighbor of g_1 are g_{L-1} and g_2 respectively. Therefore we may include (2.15) and (2.16) in one equation:

$$\tau\frac{\partial g_m(t)}{\partial t} = g_m \text{ right neighbor } + g_m \text{ left neighbor} - 2g_m \tag{2.17a}$$

$$g_0(t)=1 \tag{2.17b}$$

The set of $g_1, g_2,\ldots,g_{L-1}$ can be Fourier transformed according to the discrete Fourier transformation,

$$g_m(t)= \frac{1}{L-1}\sum_q \hat{g}(q,t)\exp(-iqL/2)\exp(-iqm) \tag{2.18a}$$

$$\hat{g}(q,t)= \sum_{m=1}^{L-1} g_m(t)\exp(iqL/2)\exp(iqm) \tag{2.18b}$$

$(q=2n\pi/(L-1),\ n=0,\pm1,\pm2,\ldots,\pm(L/2-1))$

$(m=1,2,\ldots,L-1)$

Thus (2.17a) becomes an equation for $\hat{g}(q,t)$:

$$\tau\frac{\partial \hat{g}(q,t)}{\partial t} = \hat{g}(q,t)[\exp(iq)+\exp(-iq)-2]$$

$$= -2(1-\cos q)\hat{g}(q,t)$$

$$= -\lambda_q \hat{g}(q,t) \tag{2.19}$$

where $\lambda_q = 2(1-\cos(q))$ (2.20)

Hence $\hat{g}(q,t) = \hat{g}(q,0)\exp(-\lambda_q t/\tau)$ (2.21)

Since for our initial configuration $g_m(0)=(-1)^m$, $\hat{g}(q,0)$ can be derived from (2.18b)

$$\hat{g}(q,0) = \sum_{m=1}^{L-1} (-1)^m \exp(iqL/2)\exp(iqm)$$

$$= -\frac{e^{iqL}}{\cos(qL/2)} \tag{2.22}$$

The final result for $g_m(t)$ is then

$$g_m(t) = -\frac{1}{L-1} - \frac{1}{L-1} \sum_{q\neq 0} \frac{e^{iq(L/2-m)}}{\cos(qL/2)} \exp(-\lambda_q t/\tau) \tag{2.23}$$

$$m=1,1,\ldots,L-1$$

$$q=2n\pi/(L-1),\ n=0,\pm 1,\ldots,\pm(L/2-1)$$

It is easy to see that $g_{L-j}=g_j$ is satisfied by (2.23).

As discussed above, the height of column i at time t is

$$h_i(t) = \sum_{m=1}^{i} \sigma_m(t) + h_0(t).$$

Therefore

$$\xi^2(\{\sigma\},L,t) = \frac{1}{L}\sum_{i=1}^{L} [h_i(\{\sigma\},t_n) - \bar{h}(\{\sigma\},t_n)]^2$$

$$= \overline{h_i(\{\sigma\},t_n)^2} - \bar{h}(\{\sigma\},t_n)^2$$

$$= \frac{1}{L}\sum_{i=1}^{L} \left(\sum_{m=1}^{i} \sigma_m(t)^2\right) - \left(\frac{1}{L}\sum_{i=1}^{L}\sum_{m=1}^{i} \sigma_m(t)\right)^2 \tag{2.24}$$

$$\xi^2(L,t)=<\xi^2(\{\sigma\},L,t)>$$

$$=<\frac{1}{L}\sum_{i=1}^{L}\Big(\sum_{m=1}^{i}\sigma_m(t)^2\Big)>-<\Big(\frac{1}{L}\sum_{i=1}^{L}\sum_{m=1}^{i}\sigma_m(t)\Big)^2> \tag{2.25}$$

$$\text{Term1}= <\frac{1}{L}\sum_{i=1}^{L}\Big(\sum_{m=1}^{i}\sigma_m(t)^2\Big)>$$

$$= <\frac{1}{L}[\sigma_1^2+(\sigma_1+\sigma_2)^2+(\sigma_1+\sigma_2+\sigma_3)^2+\ldots+(\sigma_1+\sigma_2+\ldots+\sigma_L)^2]>$$

$$= \frac{1}{L}\sum_{i=1}^{L-1}[ig_0+2(i-1)g_1+2(i-2)g_2+\ldots+2g_{i-1}]$$

$$= \frac{L+1}{2} + \frac{1}{L}\sum_{m=1}^{L-1}(L^2+L+m^2-2mL-m)g_m \tag{2.26}$$

$$\text{Term2}=<\Big(\frac{1}{L}\sum_{i=1}^{L}\sum_{m=1}^{i}\sigma_m(t)\Big)^2>$$

$$= < \frac{1}{L^2}\,[\sigma_1+(\sigma_1+\sigma_2)+(\sigma_1+\sigma_2+\sigma_3)+\ldots+(\sigma_1+\sigma_2+\ldots+\sigma_L)]^2>$$

$$= \frac{1}{L^2}<[L\sigma_1+(L-1)\sigma_2+(L-2)\sigma_3+\ldots+2\sigma_{L-1}+\sigma_L]^2>$$

$$=(L+1)(2L+1)/6L + \frac{1}{3L^2}\sum_{i=1}^{L-1}(2L^3+3L^2+L+i^3-3L^2i-3iL-i)g_i \tag{2.27}$$

Thus (2.25) becomes

$$\xi^2(L,t)= \frac{L+1}{12} -$$

$$- \frac{1}{L-1}\sum_{q\neq 0}\sum_{m=1}^{L-1}\frac{e^{iq(L/2-m)}}{\cos(qL/2)}[-m^3/3L^2+m^2/L+(1/3L^2-1)m]\exp(-\lambda_q t/\tau)$$

$$=\frac{L+1}{12} - \frac{1}{L}\sum_{q\neq 0}\frac{1}{\lambda_q}\exp(-\lambda_q t/\tau) \tag{2.28}$$

In obtaining the simple expression for $\xi^2(L,t)$, we have used the properties of even and odd functions and the following formulas:

$$\sum_{m=1}^{L-1} m\exp(-iqm) = -(L-1)/[\exp(iq)-1]$$

$$\sum_{m=1}^{L-1} m^2\exp(-iqm) = -(L-1)[L\exp(iq)-L+\exp(iq)+1]/[\exp(iq)-1]^2$$

$$\sum_{m=1}^{L-1} m^3\exp(-iqm) = (L-1)[(L-1)^2-3(L^2-L-1)\exp(iq)$$

$$+3(L-1)(L+1)\exp(2iq)(L^2+L+1)\exp(3iq)]/[\exp(iq)-1]^4 \qquad (2.29)$$

The structure factor $S(k,t)$ is related to ξ through (1.2.3)

$$\xi^2(L,t) = \frac{1}{L}\sum_k S(k,t)$$

where $S(k,t) = < \hat{h}(k,t)\hat{h}(-k,t) >$.

However, $S(k,t)$ can not be read off from the comparison of (1.2.3) and (2.28) because the sum in (1.2.3) is over $k=2n\pi/L$ while the values of q in (2.28) are shifted $q=2n\pi/(L-1)$.

The simplest way of evaluating $S(k,t)$ is to Fourier transform the identity

$$g_m(t) = \sigma_j\sigma_{j+m} = 2C_m(t) - C_{m-1}(t) - C_{m+1}(t) \qquad (2.30)$$

where $$C_m(t) = <(h_j-\bar{h})(h_{j+m}-\bar{h})>. \qquad (2.31)$$

The right hand side then becomes $\lambda_k S(k,t)$ while the left hand side is determined by using the solution (2.23). The result is

$$S(k,t) = \frac{L}{(L-1)\lambda_k} - \frac{1}{L-1}\sum_{q\neq 0}\frac{1}{\lambda_q-\lambda_k}\exp(-\lambda_q t/\tau) \qquad \text{for } k\neq 0 \qquad (2.32)$$

while $S(0,t)=0$, which follows from the identity $\sum_i (h_i-\bar{h})=0$. There are no singular terms in (2.32) since $\lambda_k \neq \lambda_q$ for any k or q.

We now examine (2.28) in more detail:

$$\xi^2(L,t)=\frac{L+1}{12} - \frac{1}{L} \sum_{q\neq 0} \frac{1}{\lambda_q} \exp(-\lambda_q t/\tau)$$

obviously,

$$\xi(L,\infty)=(\frac{L+1}{12})^{1/2}$$

and we see that $\xi(L,\infty)\sim L^{1/2}$ as $L\to\infty$.

If the width of the surface is of the scaling form $\xi(L,t)\sim L^{\chi}G(t/L^z)$ where $G(x)\to$const as $x\to\infty$ and $G(x)\sim x^{1/2z}$ as $x\to 0$ as has been found for the Eden model, the plot of the function $\xi(L,t)/L^{1/2}$ versus t/L^z should be a single curve for all L large enough if the exponent z is chosen appropriately. Since in our case the surface of the initial configuration is not flat (i.e. $\xi(L,0)\neq 0$), $\xi(L,0)$ must be subtracted from $\xi(L,t)$ in order to obtain the scaling form $\xi(L,t)\sim L^{\chi}G(t/L^z)$.

It may not be obvious from (2.25) that $\xi(L,t)$ has the scaling form $\xi(L,t)\sim L^{\chi}G(t/L^z)$. However we can convince ourselves by plotting $[\xi^2(L,t)-\xi^2(L,0)]^{1/2}/L^{1/2}$ against t/L^z for L=96, 192, 384 and 768 with z=2.0 (see Figure 5).

We can also show the scaling form of ξ from equation (2.28):

$$\xi^2(L,t)-\xi^2(L,0)= \int_{2\pi/L}^{\pi} dq \frac{1}{q^2} [1-\exp(-q^2 t/\tau)]. \qquad (2.33)$$

where we have approximated λ_q by q^2 since the dominant

contribution comes from small q.

Consider the formula above for two cases:

a) $t\to\infty$ at fixed L

$$\xi^2(L,t)-\xi^2(L,0)\simeq \int_{2\pi/L}^{\pi} \frac{1}{q^2}\, dq \sim [1/q]_{2\pi/L}^{\pi} \sim L$$

b) $L\to\infty$ at fixed t

Let $y=q(t/\tau)^{1/2}$. Then (2.33) becomes

$$\xi^2(L,t)-\xi^2(L,0)= (t/\tau)^{1/2} \int_{2\pi(t/\tau)^{1/2}/L}^{\pi(t/\tau)^{1/2}} dy\ (1-e^{-y^2})/y^2$$

If $t/L^2\to 0$ and t is relatively large, then the formula above becomes

$$\xi^2(L,t)-\xi^2(L,0) \sim t^{1/2} \int_0^{\infty} dy\ (1-e^{-y^2})/y^2 \sim t^{1/2}$$

Therefore we have shown that (2.33) has the scaling form $\xi(L,t)\sim L^{\chi}G(t/L^z)$ with the exponents $\chi=1/2$ and $z=2$.

The scaling property of S(k,t) can be obtained in the same way, of course. This function is more interesting since it contains more detailed information about the relaxation process. We now demonstrate the scaling form of this function analytically. Consider (2.32) for small k and large L ($L\to\infty$). Given $k=2n\pi/L$ with n fixed, the sum in (2.32) is dominated by the $q=\pm q(n)=\pm 2n\pi/(L-1)$ terms since

$$\lambda_{q(n)}-\lambda_{k(n)}= 2[1-\cos(q(n))]-2[1-\cos(k(n))]$$

$$\simeq k^2(n)-q^2(n)$$

$$= (2n\pi)^2[(\frac{1}{L-1})^2-(\frac{1}{L})^2]$$

$$\simeq 2(2n\pi)\frac{1}{L}\ \frac{1}{L^2}$$

$$= 2k^2/L \sim L^{-3} \qquad (2.34)$$

while $\lambda_q-\lambda_k \sim L^{-2}$ for other values of q. Separate the q(n) terms, we obtain

$$S(k,t)\sim \frac{1}{k^2}\ [1-\exp(-\lambda_q t/\tau)] \quad \text{as } L\to\infty \qquad (2.35)$$

which shows that S(k,t) has the scaling form

$$S(k,t)\sim k^{-2+\eta} f(k^z t)$$

with $\eta=0$ and $z=2$.

A plot of $k^2S(k,t)$ vs k^zt is shown in Figure 6 and a plot of the relaxation function $\Psi(k,t)$ vs k^zt is shown in Figure 7. In Figure 7, cases of L=48 and 96 are distinguished by different types of symbols and show us the finite size effect.

2) Nonequilibrium growth ($\lambda\neq 0$)

For nonequilibrium growth the three-spin correlation functions appearing on the right hand sides of (2.9a,b) do not cancel, in general, with each other. The loss of time reversal symmetry associated with the moving interface complicates the equations. Even two-spin correlation functions get more complicated. Let's consider the term $\langle\sigma_i(\sigma_{i+1}-\sigma_{i-1})\rangle$. In the equilibrium case we have used the property $\langle\sigma_i\sigma_{i+1}\rangle=\langle\sigma_i\sigma_{i-1}\rangle$. By examining $\langle\sigma_i(\sigma_{i+1}-\sigma_{i-1})\rangle$ we find that the property $\langle\sigma_i\sigma_{i+1}\rangle=\langle\sigma_i\sigma_{i-1}\rangle$ does not hold in the nonequilibrium case.

Suppose we take the length of the lattice to be 6 and calculate $<\sigma_i(\sigma_{i+1}-\sigma_{i-1})>$ at time $t_n=\tau$. The initial configuration is represented by $\{\sigma\}=\{1,-1,1,-1,1,-1\}$ which has $<\sigma_i\sigma_{i+1}>=<\sigma_i\sigma_{i-1}>$. At time $t_n=\tau$, a number of different configurations are possible. For equilibrium growth, the six possible configurations are $\{-1,1,1,-1,1,-1\}$, $\{1,1,-1,-1,1,-1\}$, $\{1,-1,-1,1,1,-1\}$, $\{1,-1,1,1,-1,-1\}$, $\{1,-1,1,-1,-1,1\}$ and $\{-1,-1,1,-1,1,1\}$. They appear at time $t_n=\tau$ equiprobably. $<\sigma_i(\sigma_{i+1}-\sigma_{i-1})>$ can thus be calculated . It has been verified that $<\sigma_i(\sigma_{i+1}-\sigma_{i-1})>$ equals to zero at time τ for all i (i=1,2,...,L) for equilibrium growth.

The situation is different for nonequilibrium growth. At time τ the three possible configurations (if $P_+=1$) are $\{1,1,-1,-1,1,-1\}$, $\{1,-1,1,1,-1,-1\}$ and $\{-1,-1,1,-1,1,1\}$. They also appear equiprobably, which leads $<\sigma_i(\sigma_{i+1}-\sigma_{i-1})>$ non-zero, in general. For instance, $<\sigma_5(\sigma_6-\sigma_1>=(0+2+2)/3\neq 0$.

It is unfortunate that we can not solve (2.9a,b) exactly. However, one may still conjecture the properties of the interface by relating the model, at least in an approximate way, to the field theoretic model of Kardar *et al*.

The Langevin equation used by Kardar *et al*.[15] is

$$\frac{\partial h(\vec{x},t)}{\partial t}=\nu^*\nabla^2 h(\vec{x},t)+\frac{\lambda^*}{2}(\nabla h(\vec{x},t))^2+\eta(\vec{x},t) \qquad (2.36)$$

where $h(\vec{x},t)$ is the height of the profile. The first term on the right describes relaxation of the interface by a surface tension ν^*. the second term is the lowest order nonlinear term which can appear as a result of the uniform motion of the interface, and

$\eta(\bar{x},t)$ has a Gaussian distribution with $<\eta(\bar{x},t)>=0$, and $<\eta(\bar{x},t)\eta(\bar{x}',t')>= 2D\delta^{d}(\bar{x}-\bar{x}')\delta(t-t')$.

In two dimensions, (2.36) becomes

$$\frac{\partial h(x,t)}{\partial t}=\nu^{*}\nabla^{2}h(x,t)+\frac{\lambda^{*}}{2}(\nabla h(x,t))^{2}+\eta(x,t) \qquad (2.37)$$

The slope of the interface is denoted by f(x,t):

$$f(x,t)= \frac{\partial h(x,t)}{\partial x} \qquad (2.38)$$

We differentiate (2.36) with respect to x and average it over the noise to obtain

$$\frac{\partial}{\partial t}<f>_{\eta}=\nu^{*} \frac{\partial^{2}<f>_{\eta}}{\partial x^{2}} +\lambda^{*}<f\frac{\partial f}{\partial x}>_{\eta} \qquad (2.39)$$

We now show the average slope of the interface in our model obeys a similar equation.

An equation for the average slope can be obtained from the master equation (2.5). Multiply (2.5) by σ_i and sum over all possible configurations $\{\sigma\}$ and note that $<\sigma_i>= \sum_{\{\sigma\}} \sigma_i P(\{\sigma\},t)$. We obtain

$$2\tau\frac{\partial}{\partial t}<\sigma_i>= <\sigma_{i+1}>+ <\sigma_{i-1}>- <\sigma_i>+ \lambda<\sigma_i(\sigma_{i+1}- \sigma_{i-1})> \qquad (2.40)$$

Replacing the finite differences by derivatives we obtain

$$\frac{\partial}{\partial t}<\sigma(x,t)>= \frac{1}{2\tau} \frac{\partial^{2}<\sigma>}{\partial x^{2}}+ \frac{\lambda}{\tau}<\sigma\frac{\partial \sigma}{\partial x}> \qquad (2.41)$$

and one can see a term by term agreement between (2.39) and (2.41).

We further argue that our model has the distinguishing features of the field theoretic model:

1) the particles are deposited in the valleys and evaporate from the peaks which is essentially a surface tension driven relaxation process producing the $\partial^2 h/\partial x^2$ term in (2.36);

2) non-zero velocity is responsible for the $(\frac{\partial h}{\partial x})^2$ in (2.36);

3) the property $\int_0^L \frac{\partial h}{\partial x}\, dx=o$ is reflected in our model by the conservation of total magnetization and no other obvious conservation laws exist.

Since there is a close resemblance of these two models, we expect that our model has the same scaling properties as that of the field theoretic model. Kardar *et al*. studied (2.36) using a dynamic renormalization group technique. They found three different universality classes (or three fixed points in the parameter space). The fixed point $\lambda^*=0$ and $\nu^*=0$ corresponds to the random deposition model and obviously can not be reached in the parameter space of our model. The fixed point $(\lambda^*=0, \nu^*\neq 0)$ corresponds to our equilibrium growth, which gives the exponents $(\chi,z,\eta)=(1/2,2,0)$. The fixed point $(\nu^*\neq 0, \lambda^*\neq 0)$ determines the universality class $(\chi,z,\eta)=(1/2,3/2,0)$ which a moving interface belongs to. This expectation is supported by the results of Monte Carlo simulations presented in Chapter III.

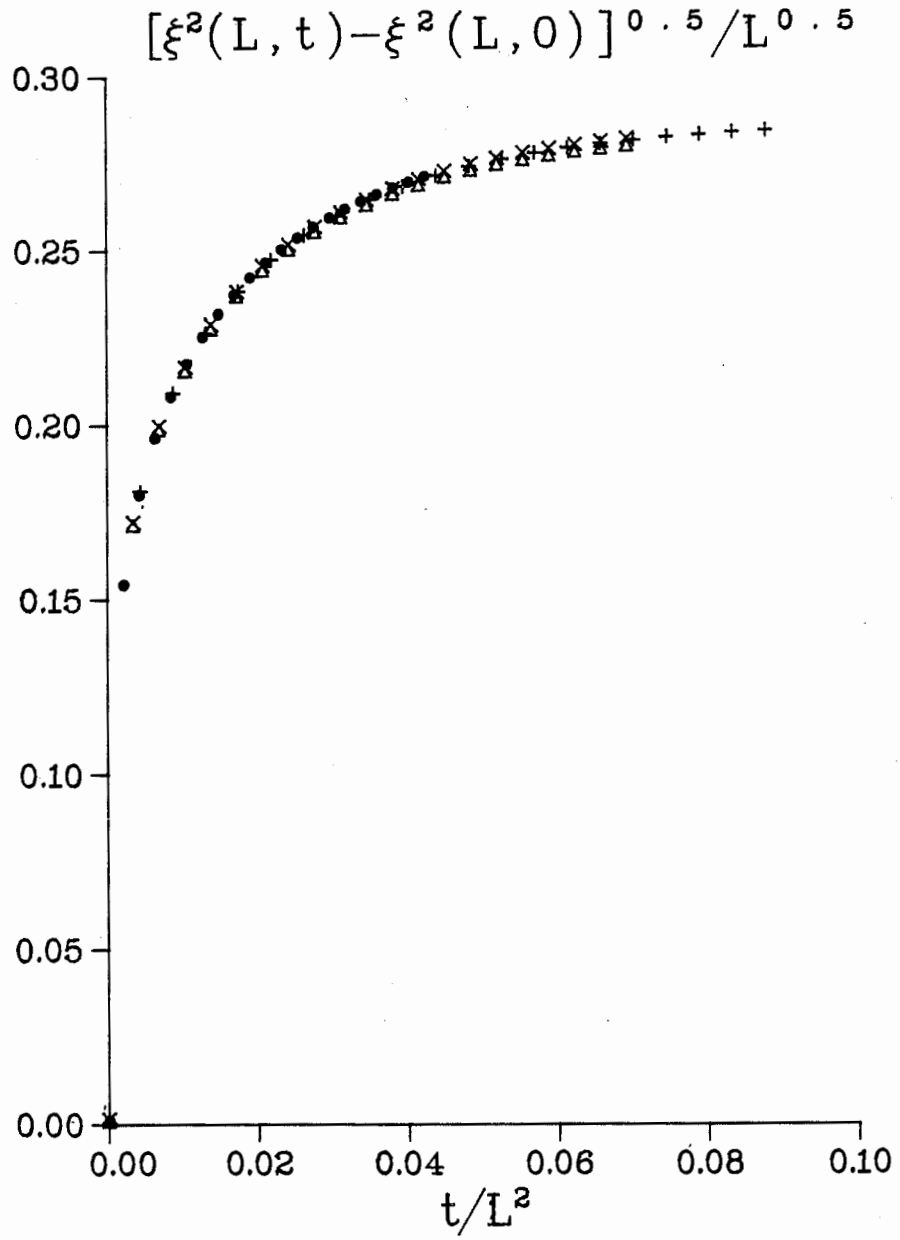

Figure 5: Analytical calculations of $[\xi^2(L,t)-\xi^2(L,0)]^{1/2}/L^{1/2}$ from (2.28) for the equilibrium growth ($\lambda=0$) regime plotted as function of t/L^z with $z=2$. Systems with L=96 (Δ), 192 (+), 384 (x) and 768 (•) are included.

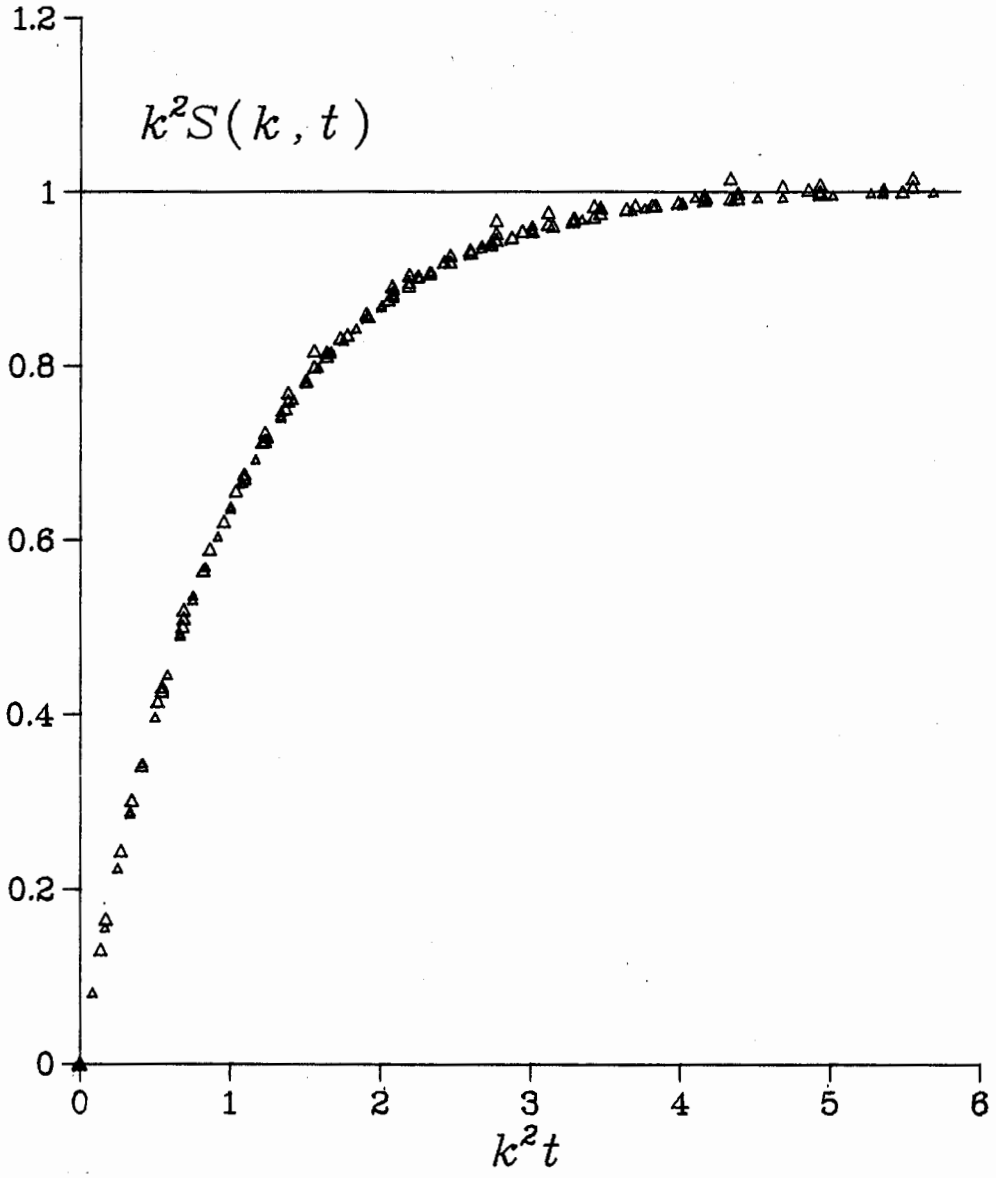

Figure 6: Analytical calculations of $k^2S(k,t)$ from (2.32) for the equilibrium growth ($\lambda=0$) regime plotted as function of k^zt with $z=2$. Systems with $L=192$, 384 and 768 are included. The data points are from the region $k<\pi/12$ of the Brillouin zone.

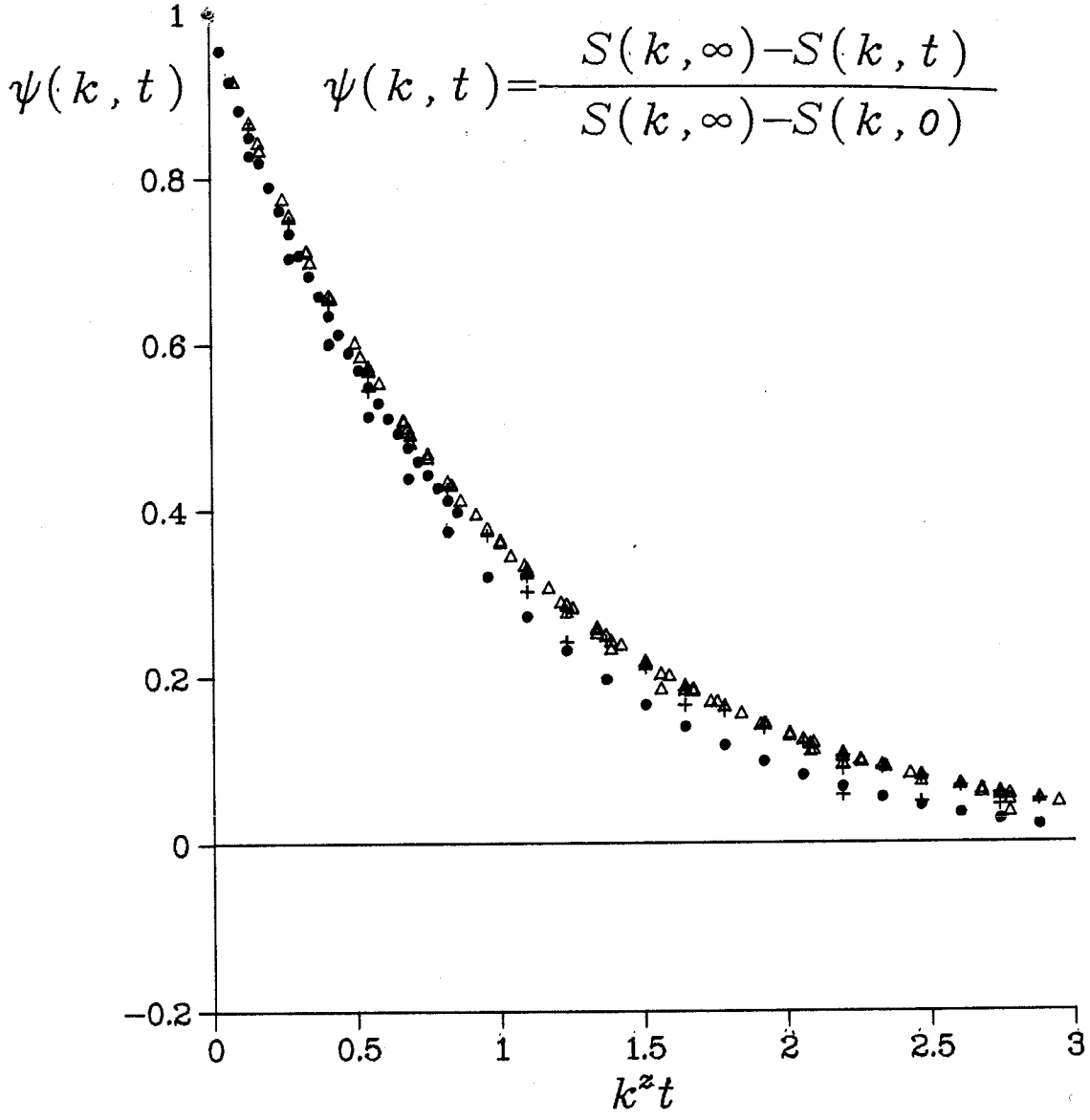

Figure 7: Analytical calculations of the relaxation function $\Psi(k,t)$ (equation (1.2.5)) for the equilibrium growth ($\lambda=0$) regime plotted as function of $k^z t$ with $z=2$. Systems with L=48 (•), 96 (+), 192 (Δ), 384 (Δ) and 768 (Δ) are included. The data points are from the region $k<\pi/12$ of the Brillouin zone. Cases of L=48 and 96 are distinguished by different types of symbols and show us the finite size effect.

CHAPTER III

SIMULATIONS AND RESULTS

The process of deposition and evaporation of particles in our model can be simulated by computer. On a strip of length L, with periodic boundary conditions applied, particles are deposited or evaporated one by one with the probabilities P_+ and P_-, respectively. The procedure is that given the probability P_+ ($P_+ + P_- = 1$) and the initial configuration of the cluster, the computer generates a random number R between 0 and 1. If $R < P_+$, a particle is dropped, otherwise a particle is evaporated. Once it has been decided whether to deposit or evaporate a particle, the computer selects a random site from all the eligible deposition sites or evaporation sites. These steps are repeated when more particles are added or evaporated. A cluster, or a sample, is formed by many particles. For each sample, one can determine various macroscopic quantities, such as $\xi(\{h\},L,t)$ and $S(\{h\},k,t)$. The average quantities of these simulated aggregates are the corresponding quantities averaged over the possible ensemble. This is realized by computer by forming enormous number of samples and averaging the interesting quantities. The more samples one generates, the more accurate the quantities are. This is limited only by the available computer time.

In the previous chapter we conjectured that the evolution of the interface could be described in terms of the dynamic renormalization group equations of Kardar *et al.*. They predicted that for any non-zero λ, $\eta=0$ and $z=3/2$, whereas for $\lambda=0$, $\eta=0$ and

z=2. We verify this for our model by first considering the scaling form of the structure factor S(k,t).

Since in the long time limit the evolution of the surface is expected to become a stationary process, we use the term "long enough time" to denote the period it takes for the process to get to stationary state. This "long enough time" is determined by examining the behavior of $\xi^2(L,t)$ or S(k,t). For example, $\xi^2(L,t)$ for L=12, P_+=1.0 is plotted in Figure 8. Any time longer than t_L is long enough for the process to reach stationary state. Of course, t_L is dependent on L and P_+.

We have investigated the behavior of S(k,t) for long times ($t\rightarrow\infty$). In Figure 9 a plot of the function $k^2S(k,\infty)$ is shown for three values of the parameter λ(0,0.5,1.0) (that is P_+(1/2,3/4,1)) and for various lengths L. In all three cases the function $k^2S(k,\infty)$ seems to approach a finite non-zero limit as k approaches zero, indicating that η is zero or at least very small. Therefore, if one assumes that η=0, the following holds

$$S(k,\infty)\sim k^{-2+\eta}$$

with η=0 for all λ.

Whether S(k,t) has the scaling form $S(k,t)\sim k^{-2}f(k^zt)$ and, if so, the value of the exponent z for various λ, can be determined by the following analysis.

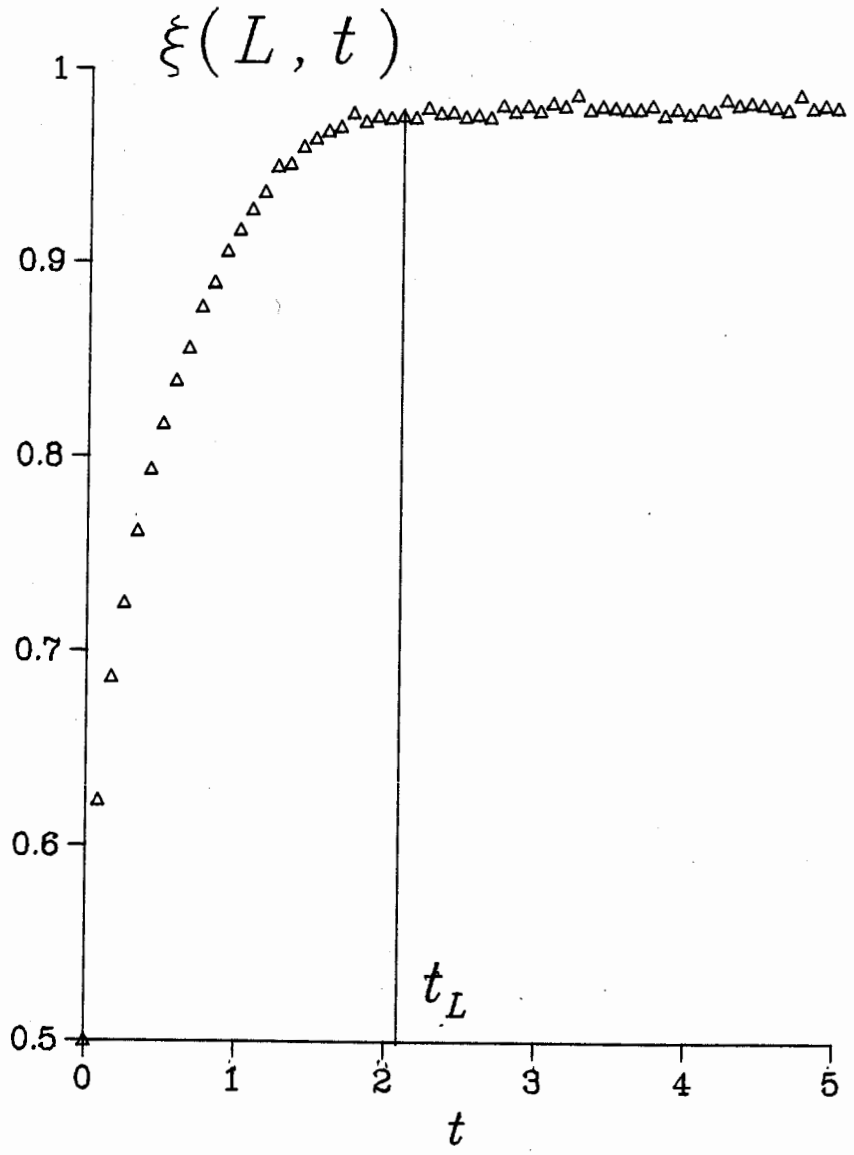

Figure 8: ξ(L,t) (L=12) for the full growth (λ=1) regime plotted as function of t, where the time scale is so chosen that t=h.

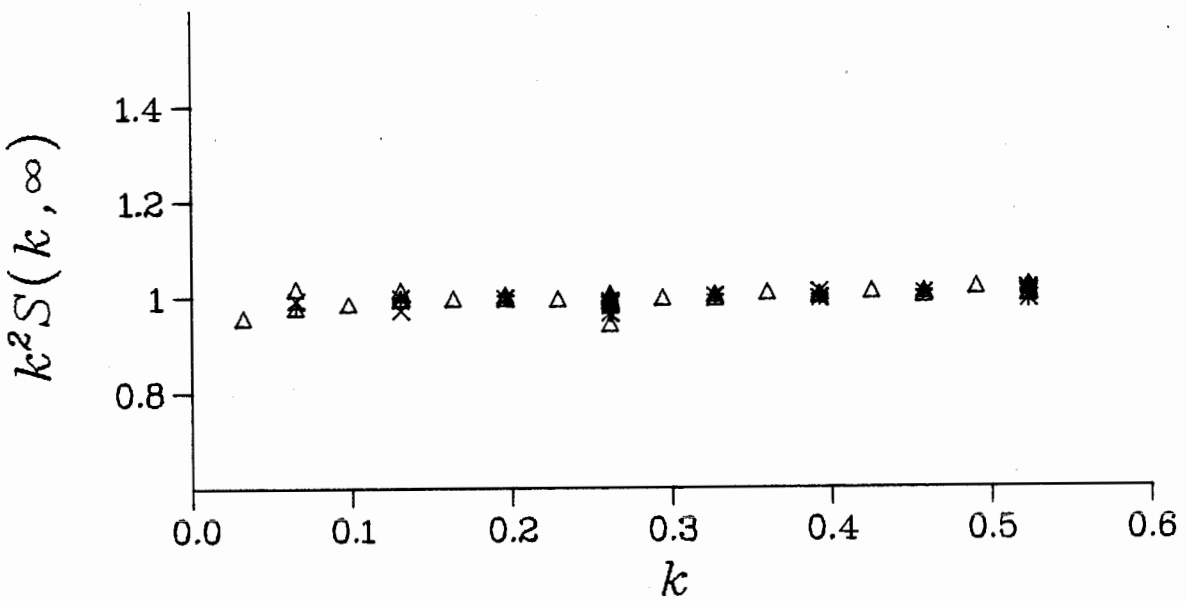

Figure 9: Steady state structure factor $S(k,\infty)$ multiplied by k^2 for the equilibrium ($\lambda=0$, denoted by +), full growth ($\lambda=1$; Δ) and the intermediate growth ($\lambda=0.5$; x) regime. The data is obtained by growing 3,000 deposits for each strip-width of L=24, 48 and 96 (L=192 has also been investigated for $\lambda=1$) and all the points with $k<\pi/6$ are displayed.

1) $\lambda=0$ $(P_+=1/2)$

This is the equilibrium case. We display $k^2S(k,t)$ as function of the scaled variable k^zt for several of the smallest k's and for various lengths L in Figure 10, where the time scale is so chosen that $t=\bar{h}=N/L$ where N is the number of total deposited and evaporated particles.

The relaxation function $\Psi(k,t)$ and the stationary state correlation function $\Phi(k,\tau)$ are displayed in Figure 11 and Figure 12, respectively. The time scale is the same as above. In both figures the data have collapsed quite precisely onto a single curve, with the exponent z=2. To compare with the simulation results, the analytical solution of $\Psi(k,t)$ is also plotted in Figure 11. The time scale of the simulation results is appropriately set (see (2.1)) that it may be plotted in the same plot of the analytical solution which comes from the continuum version of our model. Since our lengths of the strip are relatively small, we expect, as discussed for the analytical solution $\Psi(k,t)$ in Chapter II, quite strong finite size effect. However, they are quite well collapsed onto a single curve. The best estimate of z is judged by eye. By comparing the collapse of the data of $\Psi(k,t)$ when plotting $\Psi(k,t)$ against k^zt with various z, we may determine the best estimate of z and approximate error bars.

The computer simulations of the equilibrium case yield the best estimate of z to be 2.0 ± 0.1. Our analytical and simulation results match each other quite well.

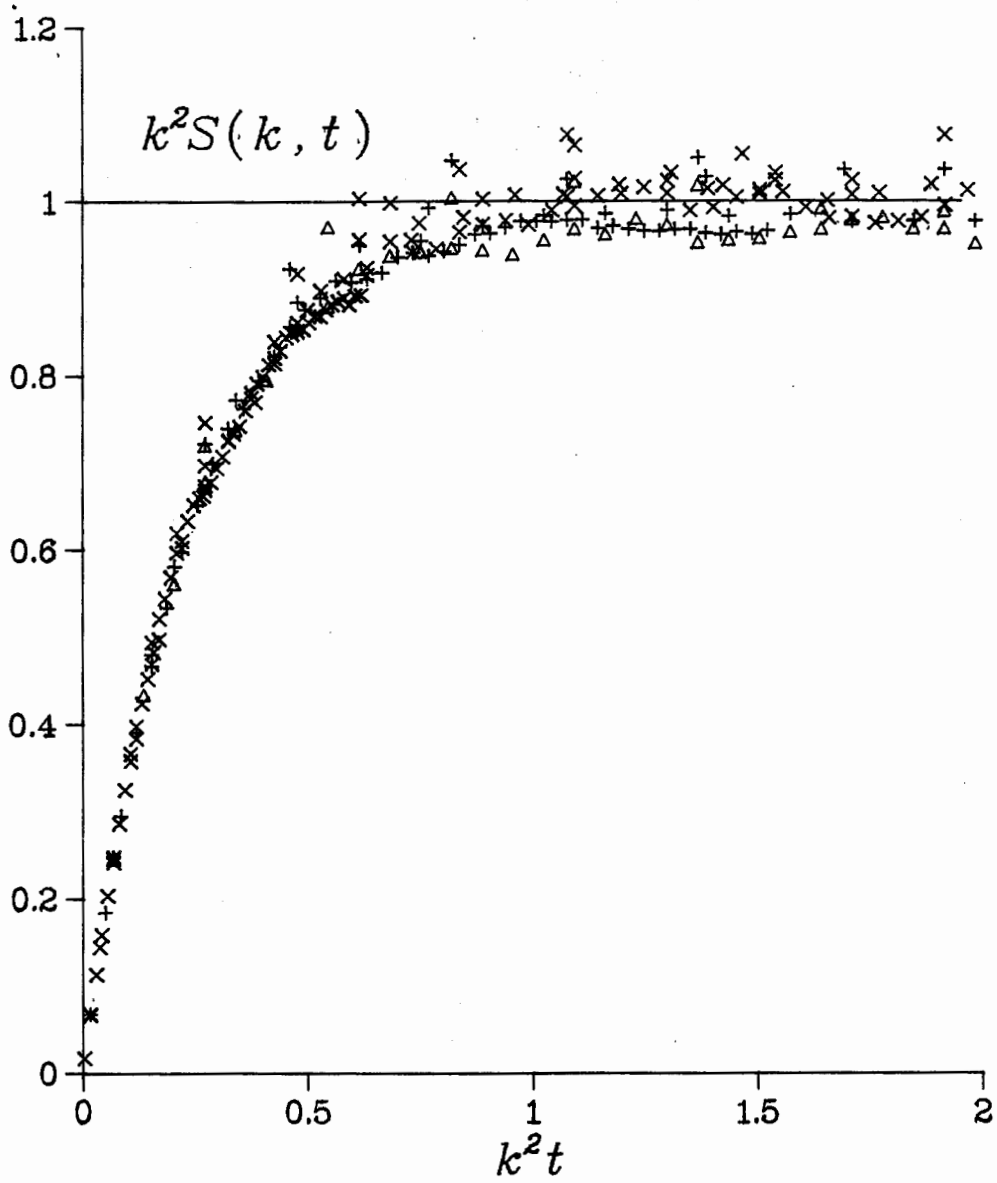

Figure 10: $k^2S(k,t)$ for the equilibrium growth ($\lambda=0$) regime as function of the scaled variable k^zt with $z=2$. Systems with $L=24$ (Δ), 48 (+) and 96 (x) are included and at least 3,000 clusters have been grown for each L. The data points are from the region $k<\pi/6$ of the Brilliouin zone.

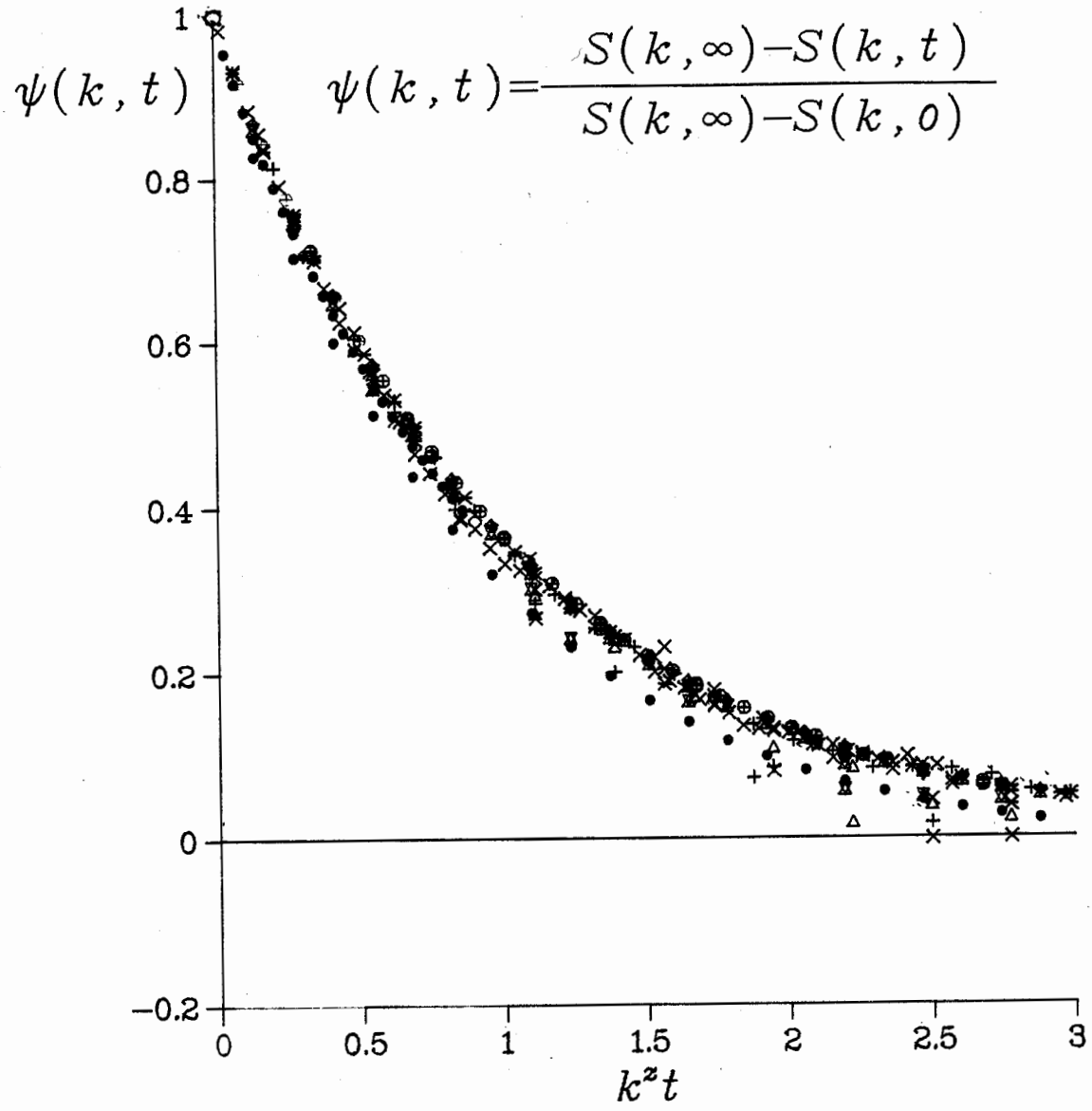

Figure 11: Relaxation function $\Psi(k,t)$ (equation (1.2.5)) for the equilibrium growth ($\lambda=0$) regime plotted as function of $k^z t$ with $z=2$. Systems with L=24 (Δ), 48 (+) and 96 (x) are included and at least 3,000 clusters have been grown for each L. The data points are from the region $k<\pi/6$ of the Brilliouin zone. Also included is the analytical calculation of $\Psi(k,t)$ (denoted by •). The time scale of the simulation results is appropriately set (see (2.1)) that it may be plotted in the same plot of the analytical solution which comes from the continuum version of our model.

2) $\lambda=1$ ($P_+=1$)

In Figure 13 and Figure 14 the relaxation function $\Psi(k,t)$ and the stationary state correlation function $\Phi(k,\tau)$ are plotted for maximum growth rate as function of the scaled variables $k^z t$ and $k^2\tau$ with $z=1.55$. This value of z produces the best collapse of the data for all these functions. The effect that the steady state correlation function separates into two universal branches has been noticed in studying the Eden model.[14] The upper branch corresponds to the smallest non-zero $k=2\pi/L$ in the Brillouin zone; the lower branch corresponds to the rest of the k's used in the plot. Both branches are quite well collapsed for a single value of z. One could also obtain the value of z by plotting $\xi(L,t)/L^{1/2}$ against the scaled variable t/L^z. However the best estimate of z comes from the relaxation function $\Psi(k,t)$ since this function probes the scaling region directly. According to our simulation data, the best estimate of z is 1.55 ± 0.1.

3) $\lambda=0.5$ ($P_+=3/4$)

We last discuss the intermediate case between equilibrium and maximum growth. Guided by what we have done successfully for equilibrium and maximum growth cases and the expectation that all cases with non-zero growth velocity belong to the same universality class of $\eta=0$ and $z=3/2$, we first plotted the relaxation function $\Psi(k,t)$ for small k's of various lengths of the strip on which the process occurs, hoping that a single value of z, expected to be about 1.5, would yield the collapse of the data. Unexpectedly, when $\Psi(k,t)$ was plotted as a function

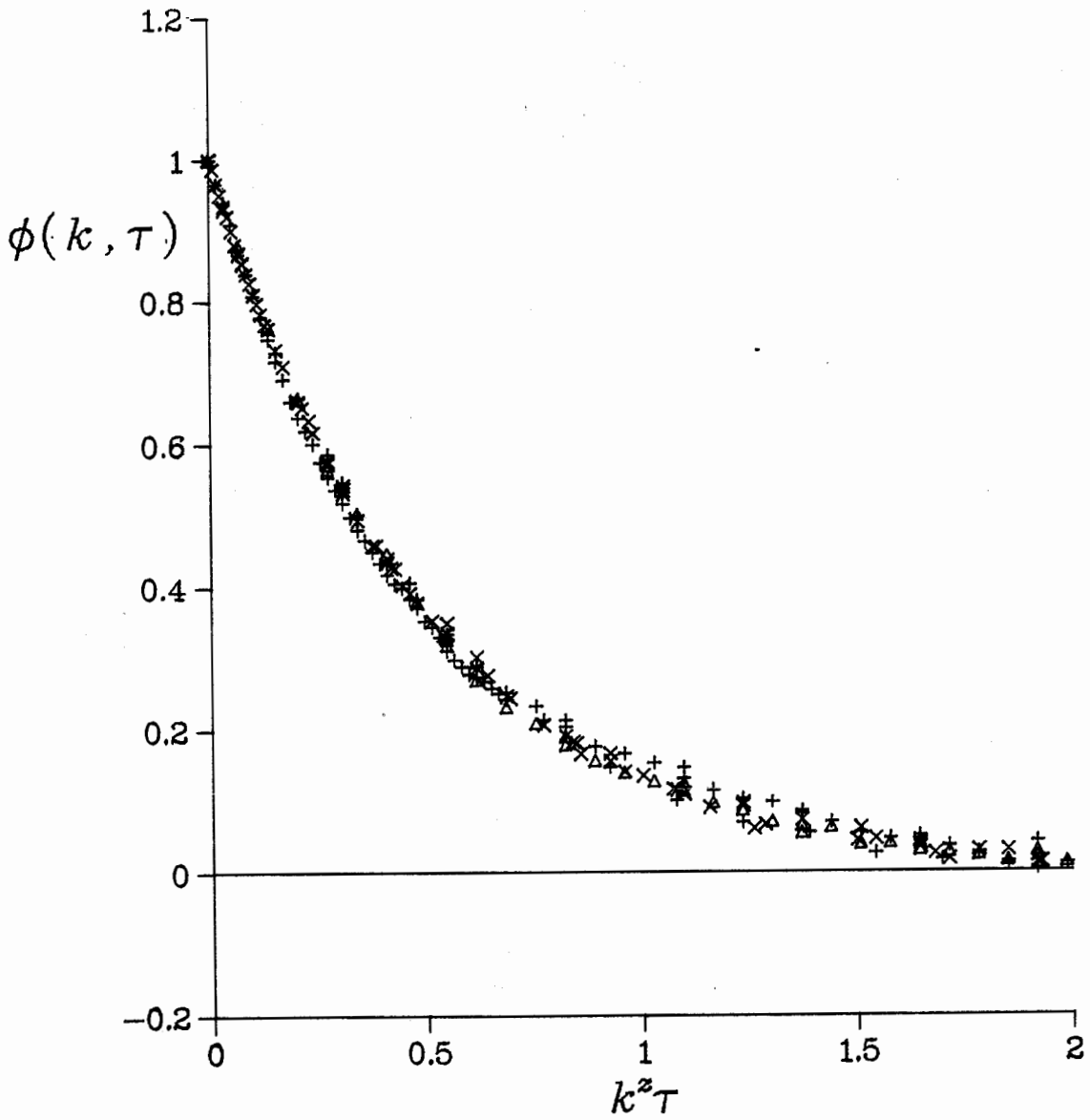

Figure 12: The steady state time-correlation function $\Phi(k,\tau)$ (equation (1.2.6)) for the equilibrium growth ($\lambda=0$) regime plotted as function of $k^z\tau$ with z=2. Systems with L=24 (Δ), 48 (+) and 96 (x) are included and at least 3,000 clusters have been grown for each L. The data points are from the region $k<\pi/6$ of the Brilliouin zone.

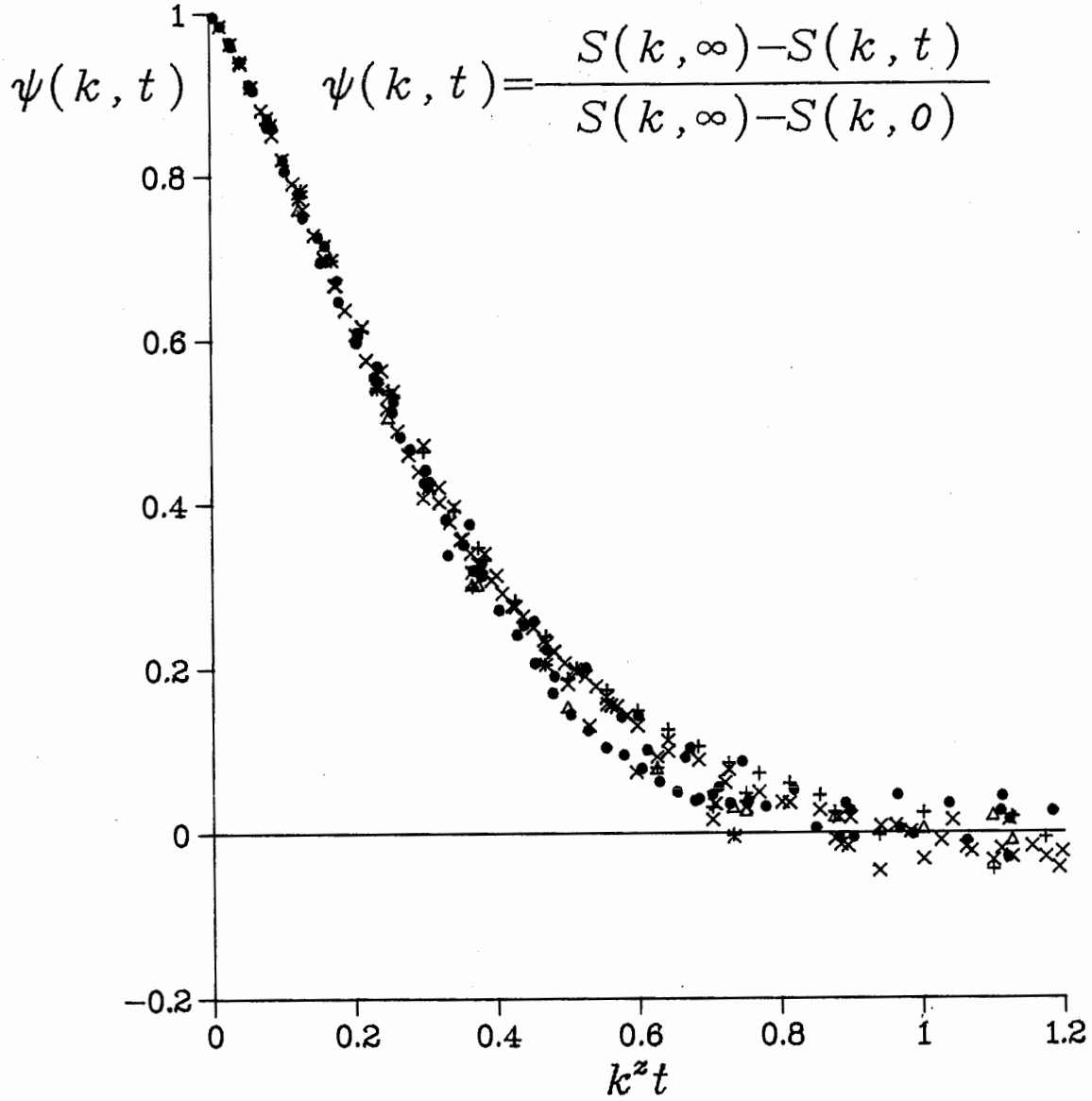

Figure 13: Relaxation function $\Psi(k,t)$ for the full growth ($\lambda=0$) regime plotted as function of $k^z t$ with $z=1.55$. Systems with L=24 (Δ), 48 (+) and 96 (x) and 192 (•) are included and the data is obtained from growing 6,000 clusters for each L=24, 48 and 96 and 3,000 deposits for L=192. The data points are from the region $k<\pi/6$ of the Brillouin zone.

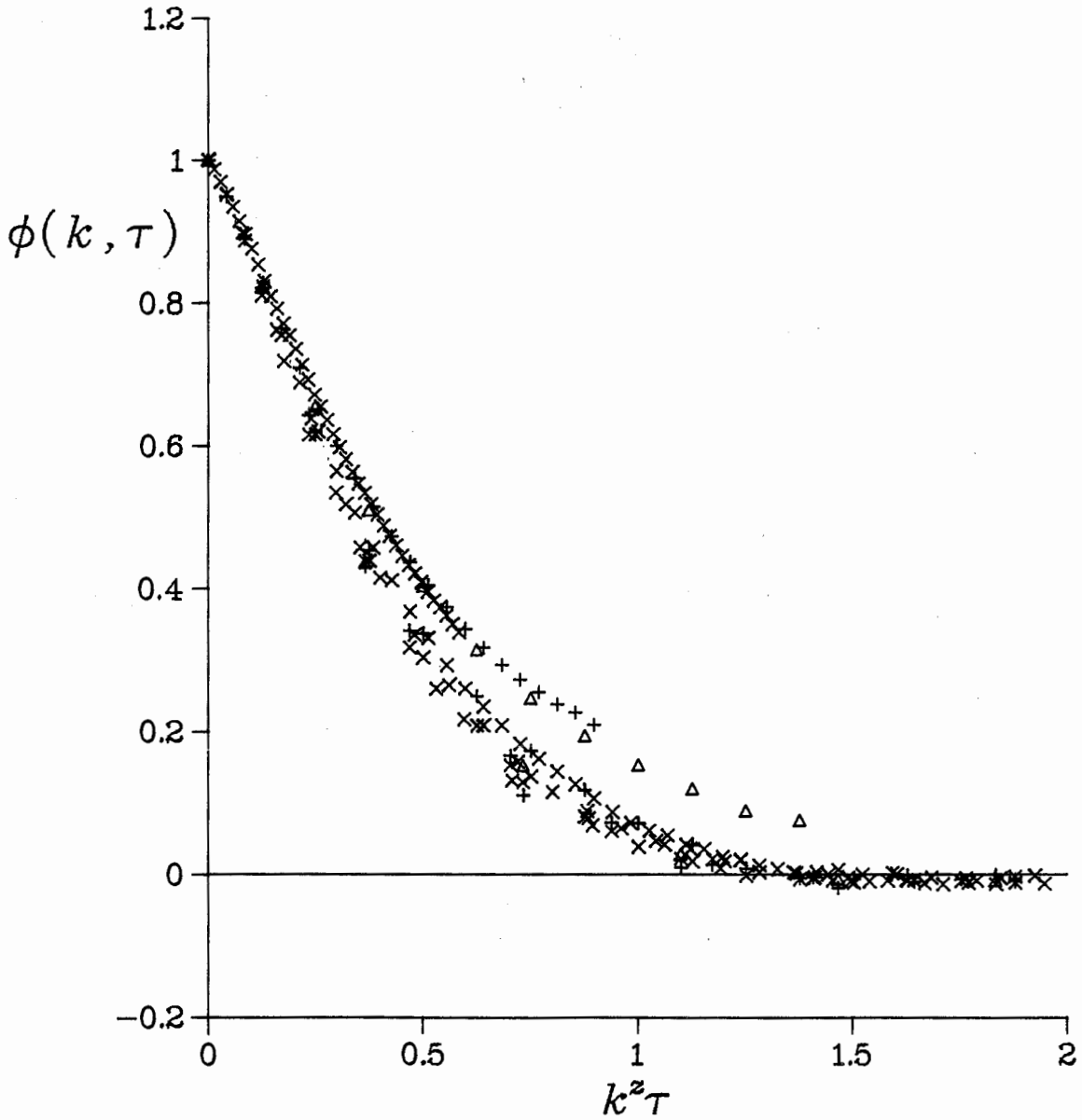

Figure 14: Same as Figure 13 but for $\Phi(k,\tau)$ for strips of width L=24, 48 and 96.

of the variable $k^z t$ for L=24, 48 and 96, the data did not fall on a single curve for any single value of z. However, when plotting $\Psi(k,t)$ vs $k^z t$ for each L separately, we found that $\Psi(k,t)$ did scale, with z dependent on L when L is relatively small. This L dependence of z is so strong, in other words, the finite size effect is so strong, that a single value of z for all L simply does not exist. We expect that if L is large enough, this finite size effect will vanish and a single value of z will be universal for all large L. Simulations for L larger than 96 were then carried out. In Figure 15,16,17,18 and 19, $\Psi(k,t)$ is plotted as function of $k^z t$ for L=48, 96, 192, 384 and 768 separately. For L=768 only 1,200 samples were generated since the simulations were very time consuming. The best collapse of the data occurred for z(48)=1.85, z(96)=1.75, z(192)=1.70, z(384)=1.65 and z(768)=1.57. One can see that z approaches 1.5 when L gets larger. The data for L=768 collapses onto a single curve fairly well even for only 1,200 samples. The curve is quite scattered but no systematic variation of the relaxation function is observed. We expect that if more samples are generated the curve will be less scattered and the larger L gets the closer z approaches 3/2.

These simulations are consistent with our analytical results and give support to the universality classification of the zero growth velocity model and the non-zero growth velocity model. Simulations yield that for zero growth velocity case the exponents η and z are 0 and 2, respectively, while η=0 and z=3/2 for non-zero growth velocity case.

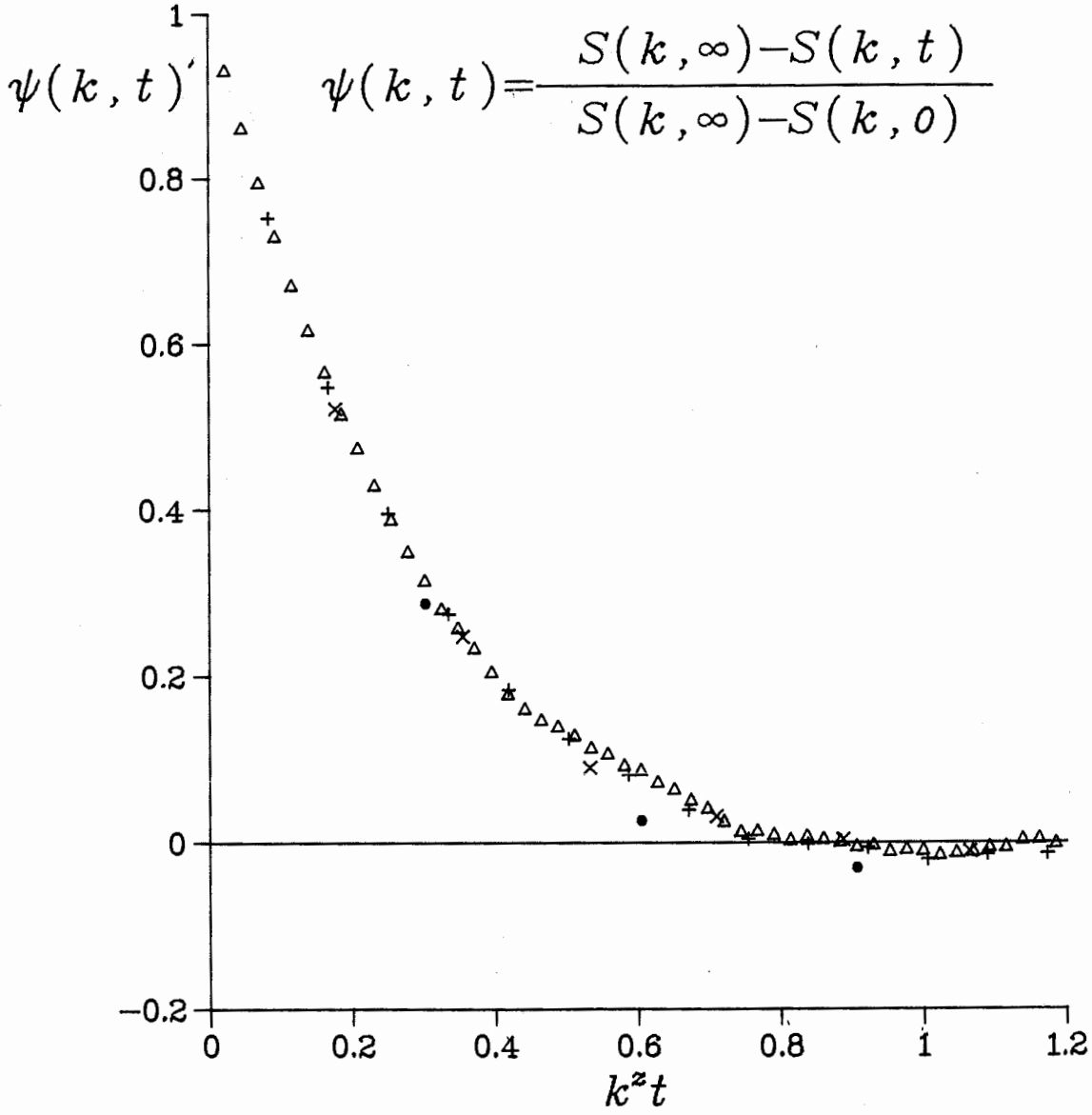

Figure 15: Relaxation function $\Psi(k,t)$ with L=48 for the intermediate growth (λ=0.5) regime as function of $k^z t$ with z=1.85. The 4 lowest values of k are included and the data is obtained from growing 9,000 clusters.

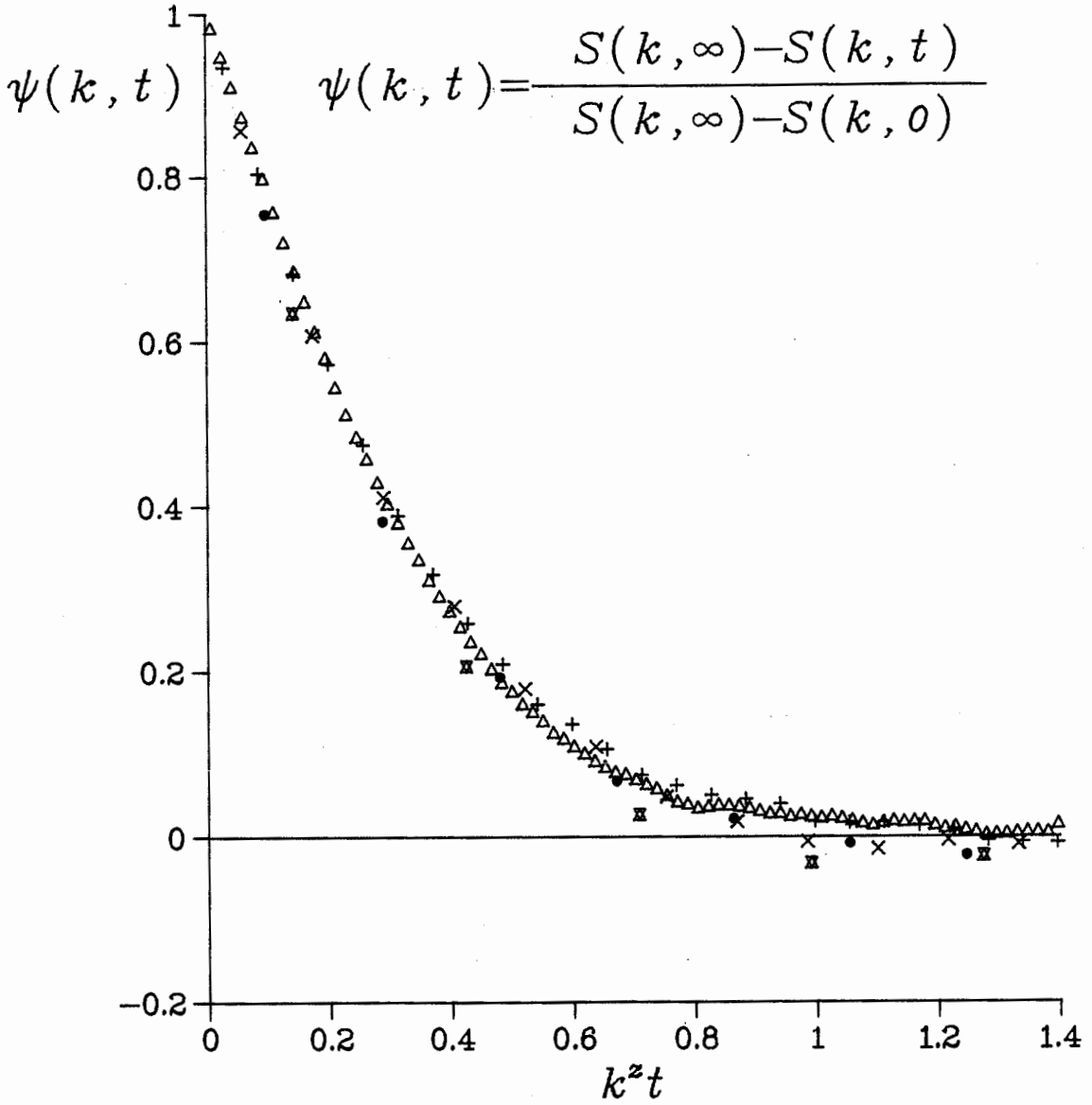

Figure 16: Relaxation function $\Psi(k,t)$ with L=96 for the intermediate growth (λ=0.5) regime as function of $k^z t$ with z=1.75. The 5 lowest values of k are included and the data is obtained from growing 9,000 clusters.

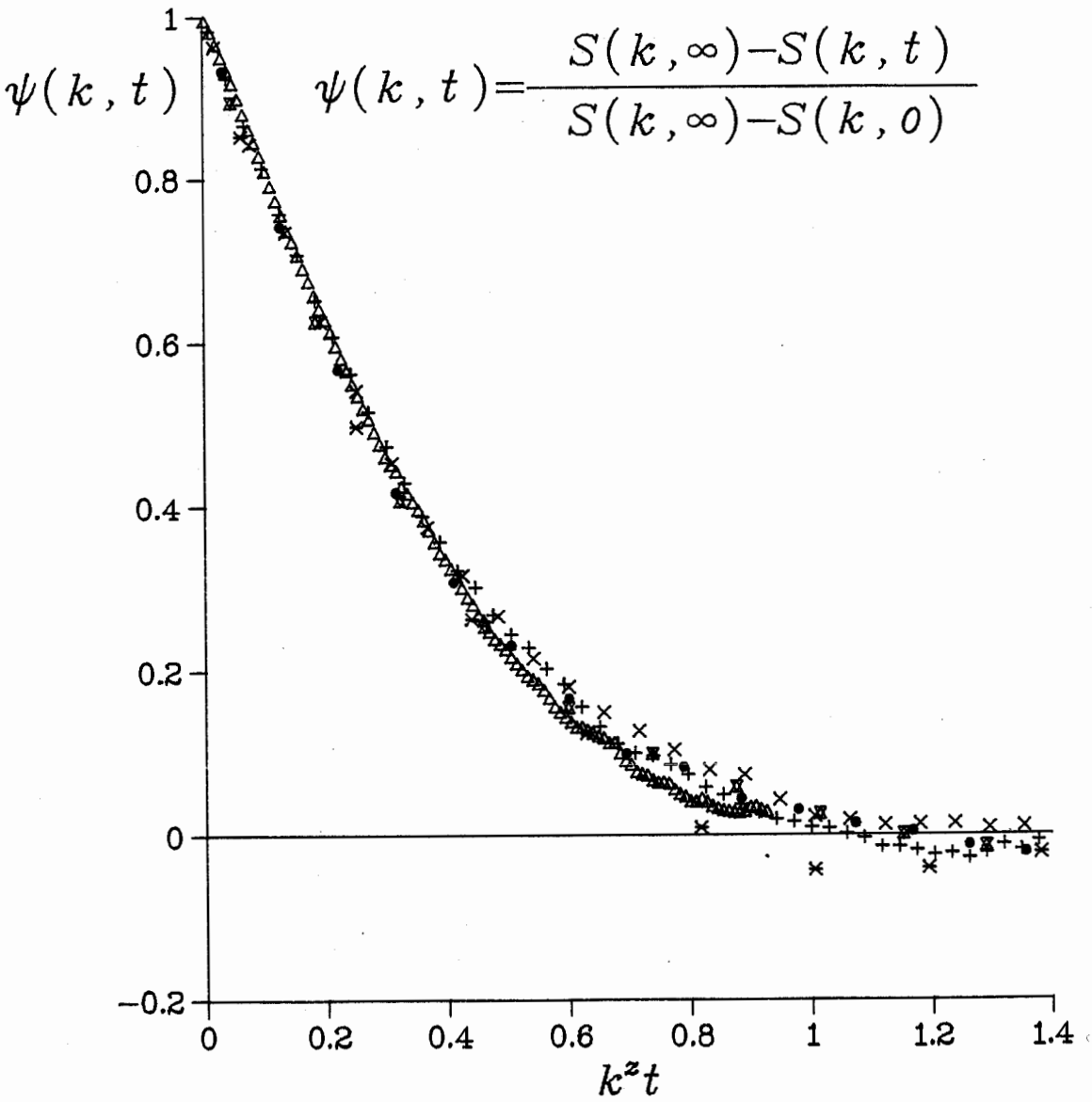

Figure 17: Relaxation function Ψ(k,t) with L=192 for the intermediate growth (λ=0.5) regime as function of $k^z t$ with z=1.70. The 6 lowest values of k are included and the data is obtained from growing 3,195 clusters.

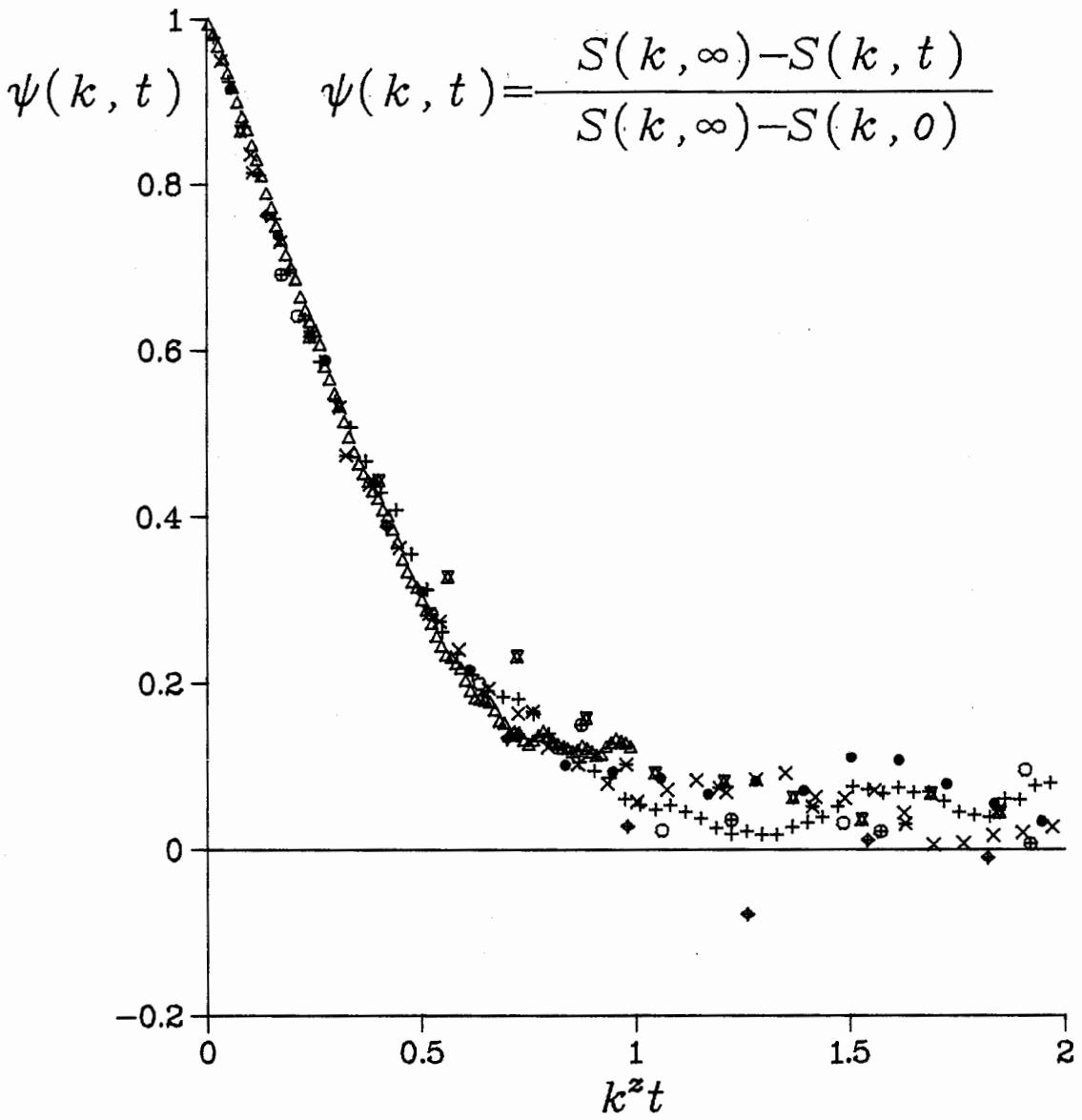

Figure 18: Relaxation function $\Psi(k,t)$ with L=384 for the intermediate growth (λ=0.5) regime as function of $k^z t$ with z=1.65. The 9 lowest values of k are included and the data is obtained from growing 1,000 clusters.

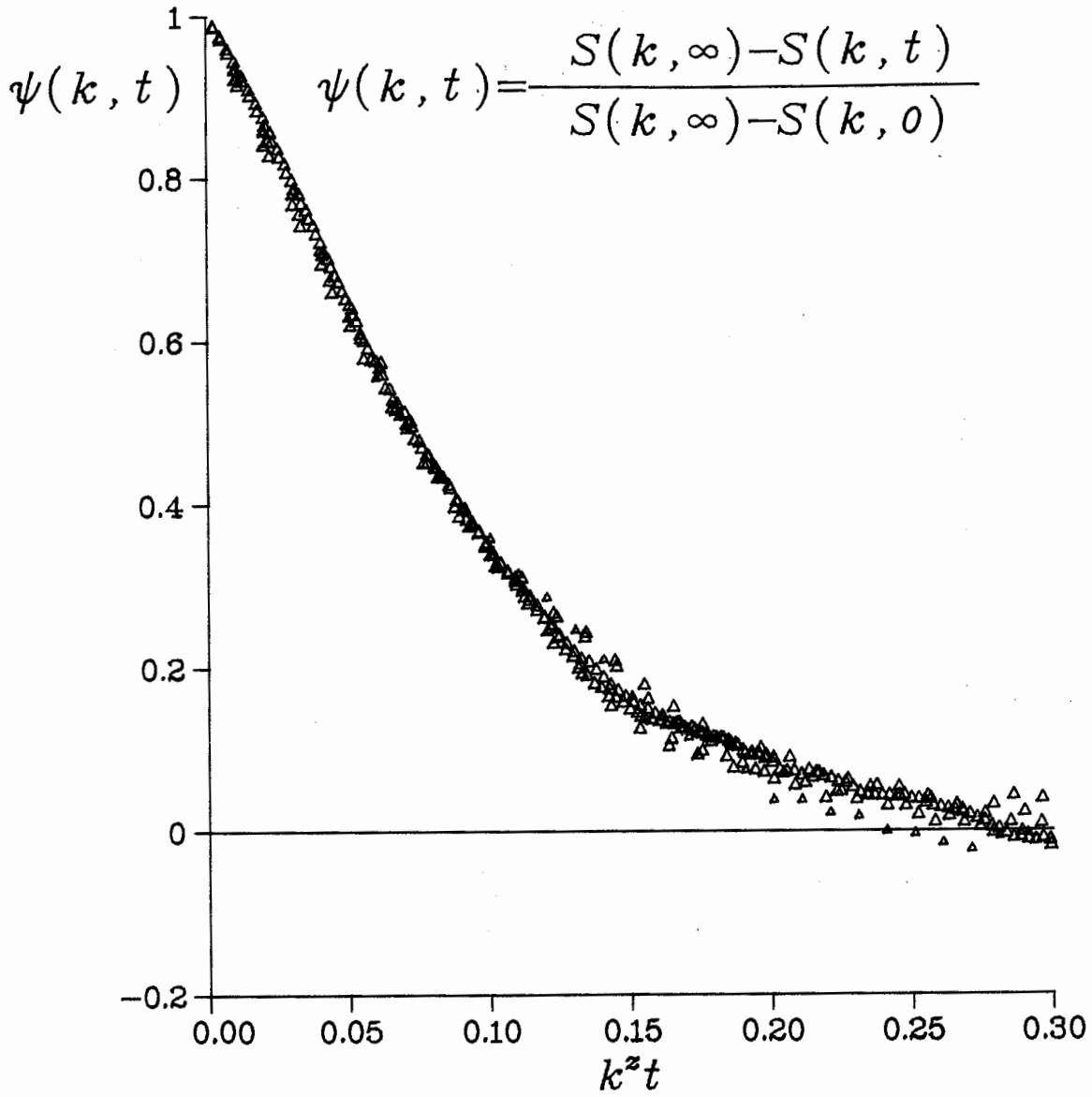

Figure 19: Relaxation function $\Psi(k,t)$ with L=768 for the intermediate growth (λ=0.5) regime as function of $k^z t$ with z=1.57. The 7 lowest values of k are included and the data is obtained from growing 1,200 clusters.

CHAPTER IV

SUMMARY

In this thesis we study a model for the evolution of the profile of a growing interface. The motivation was that this model is so simple that it is possible to obtain an exact solution and it closely resembles a field theoretic model which has been studied by renormalization group methods. These two models can be compared and the universality hypothesis could be tested.

We classify the growth processes by zero average growth velocity and non-zero average growth velocity. In Chapter II and Chapter III, we investigated the model both analytically and numerically. We conclude that our model may belong to two different universality classes depending on the control parameter. This is in agreement with the results by Kardar *et al*.. One of the universality classes is $(\chi,z,\eta)=(1/2,2,0)$. Another is $(\chi,z,\eta)= (1/2,3/2,0)$. We have found that these two classes correspond to zero average growth velocity process and non-zero average growth velocity processes respectively.

According to the universality hypothesis in the study of critical phenomena in equilibrium thermodynamics, the critical properties of many seemingly different systems are determined by the general features of the systems such as the spatial dimensionality, the symmetry of the Hamiltonian and the symmetries of the equation of motion. Our results support this

hypothesis. Firstly, our model is different in detail from the model of Kardar *et al.*. Still they belong to the same universality classes. Secondly, the change in z from 2 to 3/2 is accompanied by the breaking of time reversal invariance. The last statement needs more evidence and M. Plischke and Z. Rácz have a modified model which gives support to it. The modified model is shown in Figure 20. Particles are deposited with equal probability P_+ at any site except at local maxima of the surface at which deposition is forbidden. A particle which attempts to deposit at a local maximum is discarded. Evaporation occurs with probability $P_-=1-P_+$ at any site on the surface except at local minima. The growth rules are certainly not identical to the rules of the model we have been studying in this thesis. However Monte Carlo simulations show that the modified model has the same two universality classes of our model. Again the class z=2 appears when $P_+=1/2$. Thus we conclude that the breaking of time reversal symmetry is responsible for the change of the dynamic critical exponent z. More work could be done to give further evidence for or against our argument. For example, starting from a bulk of gathered particles, applying the Eden growth rules and allowing evaporation simultaneously, one might investigate an equilibrium and nonequilibrium Eden model.

In conclusion, we have found two universality classes of our model. The growth process for zero average growth velocity belongs to the class of $\eta=0$, $\chi=1/2$ and $z=2$. And the growth processes of non-zero average growth velocity belong to the class of $\eta=0$, $\chi=1/2$ and $z=3/2$. The time reversal symmetry in the

equilibrium growth process plays an important role. The change in the dynamic exponent z is related to the breaking of time reversal symmetry which occurs as the average growth velocity becomes non-zero.

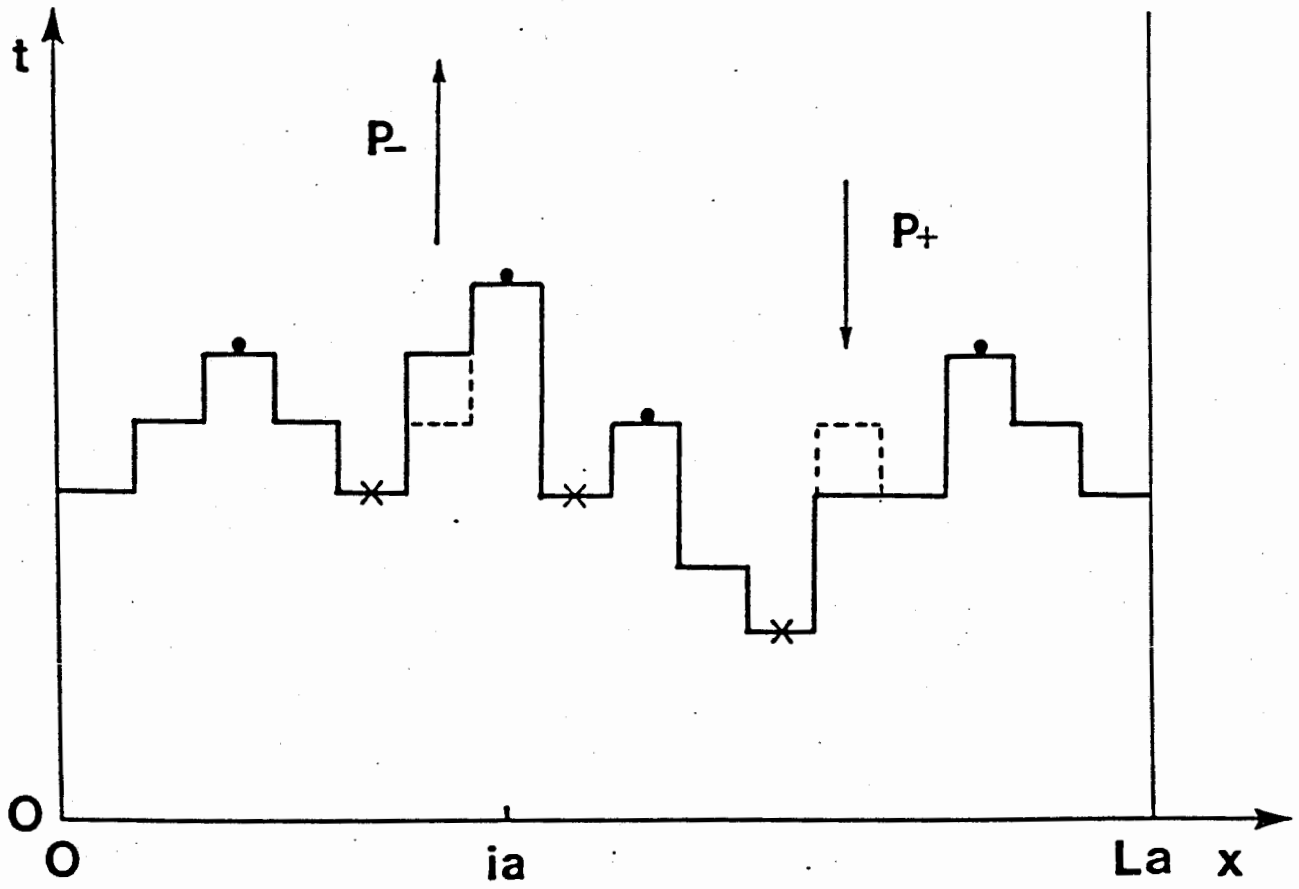

Figure 20: M. Plischke and Z. Rácz's model of interface evolution defined by deposition and evaporation events. Deposition (evaporation) occurs randomly at any site except at local maxima (minima) denoted by heavy dots (crosses) where deposition (evaporation) is forbidden. The rate of deposition and evaporation is proportional to P_+ and $P_-=1-P_+$ respectively.

BIBLIOGRAPHY

1. Kinetic of Aggregation and Gelation edited by F. Family and D.P. Laudau (North Holland, Amsterdam, 1984)

2. T.A. Witten and L.M. Sander, Phys. Rev. Lett. 47, 1400 (1981)

3. M. Eden, Proceedings of the Fourth Berkeley Symposium on Mathematics, Statistics and Probability, edited by F. Neyman, 4, 223 (1961)

4. T.A. Witten and L.M. Sander, Phys. Rev. B27, 5686 (1983)

5. L. Niemeyer, L. Pietronero, and H.J. Wiesmann, Phys. Rev. Lett. 52, 1033 (1984)

6. S.R. Forrest and T.A. Witten, Jr., J. Phys. A12, L109 (1979)

7. D.A. Weitz and M. Oliveria, Phys. Rev. Lett. 52, 1433 (1984)

8. P. Meakin and T.A. Witten, Jr., Phys. Rev. A28, 2985 (1983)

9. T.C. Halsey, P. Meakin, and I. Procaccia, Phys. Rev. Lett. 56, 854 (1986)

10. H.P. Peters, D. Stauffer, H.P. Holters, and K. Leowenich, Z. Phys. B34, 399 (1979)

11. M. Plischke and Z. Rácz, Phys. Rev. Lett. 53, 415 (1984)

12. Z. Rácz and M. Plischke, Phys. Rev. A31, 985 (1985)

13. R. Jullien and R. Botet, J. Phys. A18, 2279 (1985)

14. M. Plischke and Z. Rácz, Phys. Rev. A32, 3825 (1985)

15. M. Kardar, G. Parisi, and Yi-Cheng Zhang, Phys. Rev. Lett. 56, 889 (1986)

16. F. Family and T. Viscek, J. Phys. A18, L75 (1985)

17. M. Plischke and Z. Rácz, Phys. Rev. Lett. 54, 2056 (1985)

18. M. Kardar, G. Parisi, and Yi-Cheng Zhang, Phys. Rev. Lett. 57, 1810 (1986)

19. S.F. Edwards and D.R. Wilkinson, Proc. R. Soc. Lond. A381, 17 (1982)